MET O 11 TECHNICAL NOTE NO. 171

SOME EXPERIMENTS IN THE USE OF DIVERGENCE DAMPING IN THE OPERATIONAL ASSIMILATION MODEL

R.K. DUMELOW

Met O 11 (Forecasting Research Branch)
Meteorological Office
London Road
Bracknell
Berkshire
UK

April 1983

FH2A

CONTENTS

1. INTRODUCTION

The new operational assimilation scheme comprises a repeated insertion technique in which the models fields are successively corrected by observed data as they are integrated forward in time. At each timestep over a specified integration period (the assimilation period) the model fields are compared with observations, the differences formed and a value of the difference obtained at model grid points using the weights calculated by optimum interpolation. This increment is then scaled and inserted into the model field at the grid point. By this repeated correction procedure the model fields are forced towards the observed data, while at the same time adjustment takes place through the dynamical and physical processes in the model so that the final fields produced are in a state of dynamical balance suitable for a forecast.

When increments are inserted into the model however, locally large accelerations may be produced which may result in the generation of internal and external gravity waves, which will reveal themselves as high frequency oscillations in the model variables, particularly surface pressure. An example of how these gravity waves may be generated is illustrated in Fig 1. The figure shows how the insertion of temperature data may set up horizontal accelerations causing a wave-like perturbation in the height field.

It is undesirable to have such gravity wave motion during the assimilation period for several reasons. The example given above shows how the propagation of gravity waves can represent an adjustment away from the observed data. If gravity wave motion is present at the end of the assimilation period, then high frequency oscillations of certain model variables may continue in the subsequent forecast. Since a six hour forecast is used as a background field for the Mode 1 quality control step (comparison of observations with the background field), large amplitude oscillations in this field may cause spurious rejection of good data or spurious acceptance of bad data by the Mode 1 check.

.is is illustrated by Fig 2, which shows how a good surface pressure observation may be rejected in this way.

Another reason for wishing to eliminate gravity waves is that the small scale spatial variations they produce may result in small scale "roughnesses" on forecast charts. It is desirable to smooth out these features as they are non-meteorological in character and may result in contamination of the forecast.

This note describes two possible methods of controlling gravity waves and presents some results showing the effects of the methods on the assimilation and subsequent forecast. The results are compared with those obtained by using enhanced non-linear diffusion.

2. DIVERGENCE DAMPING

One possible approach to controlling high frequency oscillations is by the use of a conventional time filter eg Asselin (1972). This method requires three adjacent time levels of data whereas the split explicit scheme of the assimilation model needs only two levels. The extra storage required by the time filter makes the method unsuitable with current computer resources.

As indicated by the first example given in the previous section, gravity waves propagate by producing fluctuations in the divergence field. These fluctuations are generally larger than those produced by the motion of meteorological waves (Dey 1978) and damping the horizontal divergence therefore provides a way of selectively damping gravity waves. One approach to this, suggested by Bourke (1974) involves adding an artificial dissipation term $-\mu D \ (\mu > 0)$ to the divergence equation. In order to achieve this and avoid affecting the vorticity it is necessary to introduce the potential function into the momentum equations:

$$\frac{\partial u}{\partial t} = -\mu \frac{\partial \chi}{\partial x} + A_x$$

$$\frac{\partial v}{\partial t} = -\mu \frac{\partial \chi}{\partial y} + A_y$$

where A_x, A_y are the other terms in the x and y equations respectively. Since χ has to be obtained from the wind field through the solution of a Poisson equation at every timestep this method is too expensive in a primitive equation model.

(i) Conventional divergence diffusion

Another approach suggested by Shuman and Stackpole (1969) involves adding terms of the form $\mu\nabla D$ to the momentum equations:

$$\frac{\partial u}{\partial t} = \mu\frac{\partial D}{\partial x} + A_x$$

$$\frac{\partial v}{\partial t} = \mu\frac{\partial D}{\partial y} + A_y \qquad (2.1)$$

where u, v are the horizontal wind components and D the horizontal divergence. This gives the divergence equation:

$$\frac{\partial D}{\partial t} = \mu\nabla^2 D + A$$

where $A = \frac{\partial A_x}{\partial y} + \frac{\partial A_y}{\partial y}$

We will call this form of divergence damping conventional divergence diffusion or level by level divergence damping since when used in the model the divergence at each level is damped explicitly. It is the addition of the diffusion term in the divergence equation that acts to reduce divergence, whilst vorticity is unaffected. It also has the advantages of being easy and inexpensive to apply in primitive equation models. Dey (1978) however, noted that it produced in the NMC model a reduction in forecast precipitation and some anomalous flow patterns in the vicinity of mountains.

(ii) Integrated divergence damping

To overcome the problems of conventional divergence diffusion Dey proposed a modification designed to damp certain modes without producing these undesirable side effects. Following Dey, we have tried a method of damping surface pressure oscillations only and compared this with the

use of conventional divergence diffusion.

In order to understand the method proposed by Dey to control surface pressure variations, it is necessary to look at the mechanism by which such charges occur. Surface pressure changes are controlled by fluctuations in the mass divergence above the surface:

$$\frac{\partial p_*}{\partial t} = -\int_0^1 \nabla.(p_* \underline{v})\, d\sigma$$

where the symbols have their usual meaning. The integral may be re-written:

$$\int_0^1 \nabla_\sigma.(p_+ \underline{v})\, d\sigma = \int_0^1 \underline{v}.\nabla p_+ d\sigma + p_+ \int_0^1 \nabla.\underline{v}\, d\sigma \qquad (2.2)$$

The two terms on the right hand side represent changes due to advection and variations in divergence respectively. Gravity wave motions produce changes in the second integral, and damping this quantity will control resulting surface pressure oscillations. The integral may be approximated:

$$\int_0^1 \nabla.\underline{v}\, d\sigma = \sum_{k=1}^{N} \int_{\sigma_{k-\frac{1}{2}}}^{\sigma_{k+\frac{1}{2}}} D_k\, d\sigma \simeq \sum_{k=1}^{N} (\sigma_{k+\frac{1}{2}} - \sigma_{k-\frac{1}{2}})\, D_k \qquad (2.3)$$

where N is the number of levels in the vertical, D_k is the divergence on sigma surface k $(k=1,\ldots,N)$ and σ_k refers to the k-th sigma level. We define a mass weighted vertical mean divergence:

$$\overline{D}^{\sigma} = \frac{1}{p_+} \sum_{k=1}^{N} (p_{k+\frac{1}{2}} - p_{k-\frac{1}{2}})\, D_k$$

$$= \sum_{k=1}^{N} (\sigma_{k+\frac{1}{2}} - \sigma_{k-\frac{1}{2}})\, D_k \qquad (2.4)$$

Comparing (2.3) and (2.4) it may be seen that control of surface pressure oscillations due to gravity wave motion may be affected by controlling fluctuations in $\overline{D}^{\sigma}$. These are damped by applying the following equations at each level of the model:

$$\frac{\partial u}{\partial t} = \mu \frac{\partial \overline{D}^{\sigma}}{\partial x} + A_x$$

$$\frac{\partial v}{\partial t} = \mu \frac{\partial \overline{D}^{\sigma}}{\partial y} + A_y \qquad \mu > 0 \qquad (2.5)$$

We will call the use of in the diffusion term integrated divergence damping, since it is designed to damp the divergence from the column. To see the effect on column divergence, consider the divergence equation implied by (2.5):

$$\frac{\partial D_\sigma}{\partial t} = \left(\frac{\partial A_x}{\partial x}\right)_\sigma + \left(\frac{\partial A_y}{\partial y}\right)_\sigma + \mu \nabla^2 \bar{D}^\sigma$$

where σ refers to the level in question. Integrating both sides, the following equation results:

$$\frac{\partial \bar{D}^\sigma}{\partial t} = \int_0^1 \left[\left(\frac{\partial A_x}{\partial x}\right)_\sigma + \left(\frac{\partial A_y}{\partial y}\right)_\sigma\right] d\sigma + \mu \nabla^2 \bar{D}^\sigma$$

where $\bar{D}^\sigma = \int_0^1 D_\sigma \, d\sigma$ and since $\mu \nabla^2 \bar{D}^\sigma$ does not vary with σ. Hence the column divergence has been damped by the presence of the term $\mu \nabla^2 \bar{D}^\sigma$.

(iii) Non-linear diffusion

The assimilation model contains explicitly some spatial smoothing in the form of non-linear diffusion. If the variable Φ is to be affected in this way, the change due to non-linear diffusion is given by:

$$\frac{\partial \Phi}{\partial t} = K \left| \nabla^2 \Phi \right| \nabla^2 \Phi$$

where K is the diffusion coefficient. We have also compared the use of divergence damping in the assimilation with results from assimilations in which the value of the diffusion coefficient was increased fourfold.

The degree of divergence damping is determined by the value of the damping coefficient μ. The choice of this value depends on computational stability considerations, e-folding times and experimentation and this problem is dealt with in Section 4.

Dey found that integrated divergence damping had no effect upon forecast precipitation and reduced anomalous flow patterns associated with conventional divergence diffusion. The effectiveness of both forms of divergence damping as methods of noise control and the effects they have on forecast precipitation and flow patterns around mountains have been compared and contrasted with the effects of running with enhanced non-linear diffusion. The results of these experiments are presented in Section 6.

3. DIVERGENCE DAMPING IN THE ASSIMILATION PROCESS

In order to get some idea of the effect of divergence damping in the assimilation process, consider the equations of motion for an incompressible fluid with a free upper surface of height h linearised about a state of rest of height H. Following Lyne (1979), the equations are written in vorticity and divergence form with nudging terms added to represent the assimilation process. Assuming the observations satisfy the model equations and adding the divergence diffusion term, the following system results:

$$\begin{aligned}
&\frac{\partial \zeta'}{\partial t} + f D' + N_1 \zeta' = 0 \\
&\frac{\partial D'}{\partial t} - f \zeta' + g \nabla^2 h' + N_2 D' - \mu \nabla^2 D' = 0 \\
&\frac{\partial h'}{\partial t} + H D' + N_3 h' = 0
\end{aligned} \tag{3.1}$$

where $\zeta' = \zeta^o - \zeta$ etc and ζ^o etc represents and observed value.

Assuming solutions of the form:

$$\begin{pmatrix} \zeta' \\ D' \\ h' \end{pmatrix} = \begin{pmatrix} \zeta_o \\ D_o \\ h_o \end{pmatrix} e^{i(kx+ly-\upsilon t)}$$

where k, l are the wavenumbers in the x and y directions respectively, υ is frequency and ζ_o, D_o, h_o constants, then substitution into (3.1) gives the following matrix equation:

$$\begin{pmatrix} -i\upsilon+\mu(k^2+l^2)+N_2 & -f & -g(k^2+l^2) \\ f & -i\upsilon+N_1 & 0 \\ H & 0 & -i\upsilon+N_3 \end{pmatrix} \begin{pmatrix} D_0 \\ f_0 \\ h_0 \end{pmatrix} = \underline{0}$$

For non-trivial solutions the determinant must be zero, and this condition gives:

$$-f(-i\upsilon+N_3)-(-i\upsilon+N_1)\left[(-i\upsilon+\mu(k^2+l^2)+N_2)(-i\upsilon+N_3) + gH(k^2+l^2)\right]=0 \qquad (3.2)$$

Solutions to this equation for $\mu=0$ are given by Lyne (1979), and these are regarded as reference solutions. We will now consider various cases.

(i) Full update

This is the case when N_i $(i=1,2,3)$ are non-zero. Putting $N_1=N_2=N_3=N$, then (3.2) becomes:

$$(\upsilon-N_i)\left\{\upsilon^2+i\upsilon\left[\mu(k^2+l^2)+2N\right]-f^2-gH(k^2+l^2)-\mu N(k^2+l^2)-N^2\right\}=0 \qquad (3.3)$$

This gives the solutions:

$$\upsilon_1 = -N_i$$
$$\upsilon_{2,3} = -i(N+c) \pm \sqrt{\omega^2-c^2} \qquad (3.4)$$

where $\omega^2 = f^2+gH(k^2+l^2)$

$c = \frac{1}{2}\mu(k^2+l^2)$

By considering the solutions when $\mu=0$, it can be seen that the second and third solutions are high frequency gravity-inertia waves and the first solution is a stationary meteorological wave (Lyne 1979). If $\mu\neq 0$, then there are two cases to consider. For $\omega^2 \gg c^2$, the e-folding time for the gravity inertia waves is $(N+c)^{-1}$.

When $\omega^2 < c^2$, then either

$$\upsilon = -i(N+c) - ic\left(1-\omega^2/c^2\right)^{\frac{1}{2}}$$
$$= -i\left[N+c+c\left(1-\omega^2/c^2\right)^{\frac{1}{2}}\right]$$

or $$\upsilon = -i(N+c) + ic(1-\omega^2/c^2)^{\frac{1}{2}}$$

$$= -i(N+c\varepsilon)$$

where $0<\varepsilon<1$

Hence the e-folding times are $[N+c+c(1-\omega^2/c^2)^{\frac{1}{2}}]^{-1}$ and $(N+c\varepsilon)^{-1}$. The presence of the damping acts to decrease the e-folding time of the gravity-inertia waves in all cases and has no effect on the meteorological wave.

The solutions to (3.3) are plotted as a function of wavelength in Fig 3. The values of the constants used are $g = 9.81 ms^{-2}$, $f = 10^{-4} s^{-1}$, $H = 5Km$. The value of the nudging coefficient may be related to the relaxation coefficient R used for scaling increments (Obs-model) values in the assimilation. Using the one-dimensional advection equation, the relaxation process described above may be written as:

$$\frac{h^{n+1} - h^n}{\Delta t} + c\left(\frac{\partial h}{\partial x}\right)^n = N(h^{obs.} - h^{n+1}) \qquad (3.5)$$

where $h^{obs.}$ is the observed value of h, the other superscripts denote time levels, c is phase speed and a forward timestep has been used. The assimilation process in practice is given by:

$$\frac{h_+^{n+1} - h^n}{\Delta t} + c\left(\frac{\partial h}{\partial x}\right)^n = 0 \qquad (3.6)$$

$$h^{n+1} = h_+^{n+1} + R(h^{obs.} - h^n) \qquad (3.7)$$

(3.5)-(3.7) do not give a relationship between N and R. The assimilation process may be represented approximately by replacing h^n in (3.7) by h_+^{n+1}. Then by combining (3.6) and (3.7) and comparing with (3.5) after re-arrangement, the following results:

$$R = \frac{N\Delta t}{1+N\Delta t} \qquad (3.8)$$

Taking a value of $R=\phi.1$, $\Delta t=300s$ then $N\approx 0.37\times10^{-3}s^{-1}$ and this is the value taken in (3.3). Note from Fig 3 that for these values and over the range of wavelenths shown the two gravity waves have the same e -folding time $(\omega^2\gamma/c^2)$. The figure compares the effect of using three different values of μ with the undamped case $(\mu=0)$. The damping effect is greatest at shorter wavelengths where increasing the damping coefficient produces a marked decrease in e-folding times.

(ii) Wind update only

This is the case where $N_3=0$, and $N_1=N_2=N(say)$.

Making these substitutions in (3.2) gives:

$$v^3+v^2i[\mu(k^2+l^2)+2N]-v[gH(k^2+l^2)+\mu N(k^2+l^2)+N^2+f^2]$$
$$-gHNi(k^2+l^2)=0$$

The solutions to this equation are displayed in Fig 4, where -folding times are plotted as a function of wavelength. The branches of the curves correspond to the meteorological and gravity inertia waves (Lyne 1979). It can be seen from the figure that the meteorological wave is relatively unaffected by divergence damping. The effect on the gravity-inertia wave of using three different values of the damping coefficient is shown. As in the full update case, the damping effect is most marked at shorter wavelenths. The values of the constants used are $g=9.81ms^{-2}$; $H=8km$, $N=0.37\times10^{-3}s^{-1}$, $f=10^{-4}s^{-1}$.

(iii) Height update only

In this case the substitutions in (32) are $N_1=N_2=0$, $N_3=N$ giving:

$$v^3+iv^2[\mu(k^2+l^2)+N]-v[f^2+\mu N(k^2+l^2)+gH(k^2+l^2)]$$
$$-f^2Ni=0$$

The solutions to this equation over a range of wavelengths are given in Fig 5, with the constants having the same values as in the wind update case. The same qualitative effects as the wind update only case occur, with the meteorological wave being little affected but the gravity-inertia

are being damped by an amount related to the magnitude of the damping coefficient.

4. CHOICE OF DAMPING COEFFICIENT

The value of the damping coefficient μ in equations (2.1) determines the effectiveness of divergence damping with larger values decreasing the -folding time of the gravity waves to the greatest extent. However use of too large a value may produce undesirable side effects such as reduced precipitation and development, and a restriction is put on the size of the value by linear computational stability considerations. The degree to which these side effects are evident can be determined by experimentation, and the stability criterion can be obtained from a linearized version of the primitive equations with the divergence damping terms included. These extra terms do not prevent the equations from being decoupled (see Appendix) resulting in the following system:

$$\frac{\partial u_n}{\partial t} - F v_n + \frac{g}{a\cos\varphi}\frac{\partial h_n}{\partial \lambda} - \frac{\mu}{a\cos\varphi}\frac{\partial D_n}{\partial \lambda} = 0$$

$$\frac{\partial v_n}{\partial t} + F u_n + \frac{g}{a}\frac{\partial h_n}{\partial \varphi} - \frac{\mu}{a}\frac{\partial D_n}{\partial \varphi} = 0$$

$$\frac{\partial h_n}{\partial t} + \frac{c_n^2}{g} D_n = 0 \qquad n = 1, \ldots, N$$

where N is the number of model levels, (u_n, v_n, h_n) are transformed variables, c_n represents the phase speed of the n-th gravity wave, $F = f + \frac{u_n \tan\varphi}{a}$, a is the radius of the earth, and the other symbols have their usual meaning. Using centred space differencing and forward time differencing, the von Neumann method of stability analysis gives rise to the following expression as a sufficient condition for stability:

$$\mu \leq \Delta t\left(\frac{d^2}{\Delta t^2} - c_n^2\right)$$

where Δt is the timestep, d the gridlength. It can be seen that μ must decrease as c_n increases, assuming the timestep and gridlength remain constant. Hence the value for c_n chosen is that of the fastest moving gravity wave,

ıich is taken to be 311 ms^{-1} (see Appendix). Taking d to be the gridlength at 50N or S and putting $\Delta t = 300s$ gives $\mu = 3.08 \times 10^7 m^2 s^{-1}$ as a stable value. The value used operationally is 0.5×10^7 $m^2 s^{-1}$, which is thus stable according to the above criterion. Reference to the figures given in the previous section shows that this value produces acceptable e-folding times for the gravity waves ($\ll$ 6 hrs). Details of the derivation of the stability condition are given in the Appendix.

It must be noted that the gridlength increases as latitude decreases, so that higher values of μ may be used equatorward of 50°. Fig 6 shows the variations of stable values of μ with latitude.

5. DIVERGENCE DAMPING IN THE OPERATIONAL ASSIMILATION SCHEME

Divergence damping is applied at each of the adjustment steps of the integration. This may be represented by:

$$\psi_0^{t+\Delta t/3} = B(\psi^t) + D(\psi^t)$$
$$\psi_0^{t+2\Delta t/3} = B(\psi_0^{t+\Delta t/3}) + D(\psi^{t+\Delta t/3})$$
$$\psi_0^{t+\Delta t} = B(\psi_0^{t+2\Delta t/3}) + D(\psi_0^{t+2\Delta t/3})$$
$$\psi^{t+\Delta t} = A(\psi_0^{t+\Delta t})$$

where the integration operators A, B are for the advective and adjustment steps respectively and D is the contribution due to divergence damping. In the case of integrated divergence damping, $\overline{D}^o$ in (2.4) is calculated for each column, and the terms $\frac{\mu}{a\cos\varphi}\frac{\partial \overline{D}^o}{\partial \lambda}$, $\frac{\mu}{a}\frac{\partial \overline{D}^o}{\partial \varphi}$ added to the equations at each level. In the case of conventional divergence diffusion the terms added are $\frac{\mu}{a\cos\varphi}\frac{\partial D_o}{\partial \lambda}$, $\frac{\mu}{a}\frac{\partial D_o}{\partial \varphi}$ where D_o is the divergence at the level in question. In both cases, the damping is applied at all points in the horizontal, and $\mu = 0.5 \times 10^7 m^2 s^{-1}$.

6. EXPERIMENTS AND RESULTS

In order to compare the effects of divergence damping and enhanced diffusion various experiments were performed. Each experiment consisted of a 6 hr assimilation followed by a 24 hour forecast. Main run data from 12z on

ch November 1982 was used. The experiments were:

(1) Control (operational assimilation and forecast as at mid-December 1982).

(2) Enhanced non-linear diffusion during assimilation (diffusion coefficient 8×10^{14}).

(3) Integrated divergence damping with enhanced damping coefficient during assimilation.

(4) Conventional divergence diffusion during assimilation (level by level damping) with $\mu = 0.5 \times 10^7 m^2 s^{-1}$.

The assimilation in (1) and (2) contained integrated divergence damping with $\mu = 0.5 \times 10^7 m^2 s^{-1}$, whilst for the assimilation in (3) μ was allowed to vary with latitude from 0.5×10^7 $m^2 s^{-1}$ poleward of 60° to a maximum value of 5×10^7 $m^2 s^{-1}$ at the equator. The assimilations all contained non-linear diffusion with the diffusion coefficient for all variables of 2×10^{14}, with the exception of (2) for which the diffusion coefficient was 8×10^{14}. Integrated divergence damping was applied during the first six hours of each forecast except (4) with μ decreasing smoothly to zero during this time. In the case of (4) conventional divergence damping was used. All the forecasts contained non-linear diffusion with a diffusion coefficient of 2×10^{14}.

The runs were assessed according to the following criteria:

(i) The degree of "balance" achieved by the assimilation as indicated by gravity wave activity during the assimilation period and subsequent six hour forecast.

(ii) The fit of the assimilation to the observed data.

(iii) The skill of the 24 hour forecast following each assimilation.

The first two points have to be considered together as a very close fit to the observed data may imply an unbalanced initial state for the forecast causing generation of gravity waves which may contaminate the forecast itself and adversely affect the quality control step of the next analysis.

(i) Balance

As mentioned previously gravity waves propagate by high frequency fluctuations in the divergence field. One variable which is sensitive to changes in the column divergence is the surface pressure and variations in this quantity is a measure of external gravity wave propagation. The surface pressure at 45°N 0°E is plotted as a function of time during the assimilation in Fig 7. The lines on the graph correspond to the four experiments run, with an extra curve for the case of no divergence damping. It can be seen that this curve corresponds very closely with the control run curve and that for (3), suggesting that integrated divergence damping here with $\mu = 0.5 \times 10^{7} m^{2} s^{-1}$ has little effect on the assimilation and increasing the damping coefficient has only negligible benefit. On the basis of this result we will now consider only experiments (1), (2) and (4).

Refering back to Fig 7, it can be seen that small amplitude oscillations remain in the control run at the end of the assimilation period, whereas these are damped by run (4) but little affected by enhanced diffusion. The corresponding curves for the subsequent six hour forecast are given in Fig 8. It can be seen from this that (4) has least oscillations in p_s , but rather surprisingly in this case all the curves have a similar shape at the end of the forecast period.

A global measure of oscillations of p_s is given by the global RMS pressure tendency. This is plotted as a function of time for assimilation and following 6 hour forecast in Figs 9 and 10. Enhanced diffusion makes little impact on the RMS pressure tendency, whilst the use of conventional divergence diffusion produces a marked decrease during the assimilation. These trends are maintained during the 6 hour forecast, as illustrated in Fig 10. All curves show a slight increase initially in the forecast period as the forcing of the assimilation is removed.

Another measure of gravity waves of "noise" in the model is given by the global RMS divergence, which is plotted for assimilation and forecast in Figs 11 and 12. Enhanced diffusion causes a slight decrease in this quantity during the assimilation whereas conventional divergence diffusion produces a very marked decrease initially tailing off to a value considerably lower than in the control run. During the following 6 hour forecast, the RMS divergence in the control run continues to fall slowly where as the forecasts from assimilations with enhanced diffusion and conventional divergence diffusion produce a steadily increasing RMS divergence.

The fact that RMS divergence is reduced in experiment (4) suggests that internal gravity waves are being damped. In figures 13, 14 and 15 the height of certain sigma surfaces at 45N OE are plotted as a function of time during the assimilation period. The height of a sigma surface changes in response to changes in surface pressure and to changes in divergence above the surface which may be caused by internal gravity waves. Comparison of the control runs between Figs 13-15 and Fig 7 shows that fluctuations in height of the sigma surfaces are not exactly in phase with variations in the surface pressure at the same point, and therefore indicate the presence of internal gravity waves. The effect of the conventional divergence diffusion is to control the oscillations in heights by the end of the assimilation period (see Fig 15) thus reducing internal gravity wave activity.

(ii) Fit to data of assimilation

A measure of the fit of the assimilation to the observed data is given by RMS values of the difference between observed and assimilated values at observation points. The global RMS statistics for each experiment and each variable are given in Table 1. Enhanced diffusion gives an improved fit to data over the control run, but the use of conventional divergence diffusion gives a better fit and in particular, an improvement

of 0.6 knot in the RMS wind values is achieved. Table 2 (i) gives RMS errors for each variable for a mid-latitude band in the northern hemisphere and between pressure levels 350 mb and 156 mb. This region of the model atmosphere should include the main jet streams. It can be seen that the lowest RMS wind values are attained by experiment 4.

Despite noticeable differences in RMS errors between the three runs, large differences do not appear on charts in most areas. As an illustration of this the MSLP and 250 mb wind charts from experiments (1) and (4) are shown in Figs 16, 17, 18, 19. The centres of certain features taken from the hand analysed chart at the corresponding time are marked or the MSLP charts, and areas of winds with strengths over 60 knots and certain spot values are shown. Conventional divergence diffusion does not appear to reduce the strength of the jets in this case, but in fact appears to produce a slightly better correspondence with the hand analysed charts, particularly over the eastern part of the USA. The biggest difference between the two runs can be seen in the tropical 250 mb wind charts, shown in Figs 20-25. Observed winds at the same level are shown in Fig 26 for comparison. The result of conventional divergence diffusion is to produce a considerably smoother wind field throughout the tropical region. In particular an area of spurious, strong winds blowing off the south-west coast of Celebes evident in the control run is eliminated in the run with conventional divergence diffusion. Additional evidence of the increased smoothing can be seen by comparing areas in the Arabian sea and over eastern and central Africa.

The improved fit to the observations suggested in Table 2 is confirmed in the equatorial region by comparison of the observed to model winds in Figures 21 to 26, and by the RMS errors given in Table 2 (ii).

(iii) Fit to date of 24 hour forecast

The main aim of making improvements to the assimilation is to produce improvements in the subsequent forecasts. Global RMS errors for a 24 hour

forecast for three of the experiments is given in Table 3.

The best fit to data is once again achieved by the run with conventional divergence diffusion with the most marked improvement occurring in the wind field. Table 4 gives the RMS errors for a mid-latitude band.

7. DISCUSSION

There are reasons why it is to be expected that increasing the amount of smoothing or damping in the operational assimilation will improve the fit to observations as measured by RMS differences at observation points. If gravity waves persist throughout the assimilation period then small scale spatial variations or "roughnesses" may appear in the final fields resulting in a poor agreement between assimilated values and observations. This is illustrated in Fig 27, where u is plotted at a number of adjacent grid points at latitude 60°N. Values from the three runs are plotted as well as the profile from the optimum interpolation, which is taken as a reflection of the observed data. It can be seen that the large horizontal shear in u occuring in the control run is smoothed out by both the increased diffusion and divergence damping giving a better fit to the OI profile.

When data is inserted into the model imbalances may be set up as a result of observations differing from the model field significantly or as a result of noise in the observations themselves. These imbalances are reduced through mutual adjustment of mass and wind to a state consistent with the observations and by the generation of gravity waves. As was illustrated by Fig 1, gravity waves may represent an adjustment away from the observations. Control of them by divergence damping should therefore improve the fit to data. This hypothesis is supported by the global RMS values, which decrease in the run with divergence damping. The problem seems likely to be more acute when mass data is to be assimilated in the tropics where the coupling between mass and wind fields is small. Suppose, for example, that the assimilation is required to raise pressure

at the centre of a high, then the outflow subsequently produced will be prevented to only a small extent by the Coriolis force. This mechanism may also account for roughnesses in the tropical wind field, since winds produced as a result of outflows or inflows in areas where mass data is inserted may be inconsistent with those observed in nearby areas. Hence control of divergence should produce smoother wind fields in the tropics, as is shown by Figures 20-25.

8. SIDE EFFECTS

The undesirable consequences of conventional divergence diffusion as reported by Dey (1978) in the NMC model were anomalous flow patterns in the vicinity of mountains and reduced precipitation in the forecast. None of the runs performed were observed to produce spurious flow patterns in the vicinity of mountains, even though particular care was taken to check the main mountain masses such as the Himalyas, Andes and Rockies.

Time series of values of global mean dynamic and convective rainfall produced during the assimilation are plotted in Figs 28 and 29. Results from experiments (1) and (4) are shown. The dynamic accumulations are reduced significantly by divergence damping (by reducing vertical motions) whereas convective totals have been reduced to a lesser extent. Despite this reduction in rainfall totals, subsequent forecasts have not showed unrealistic overall rainfall reductions.

Neither forms of divergence damping appear to have had any effect on the development of meteorologically significant features: There has been no observed systematic filling of lows, declining of highs or reducing or increasing of jet strengths occurring in experiment (4) compared with (1).

The effects on rainfall and flow patterns of conventional divergence diffusion seem to be considerably less than those reported by Dey. This may in part be explained since Dey uses $\mu = 10^8 \, m^2 s^{-1}$ whilst the value used here is $0.5 \times 10^7 \, m^2 s^{-1}$.

9. SUMMARY AND CONCLUSIONS

Experiments have been run with the operational assimilation model to see the effects of increasing non-linear diffusion, increasing the amount of integrated divergence damping, and using conventional divergence diffusion in which the divergence at a particular level is damped directly. Increasing the integrated divergence damping has little effect on the assimilation, whereas the other two methods both have some favourable impact. The greatest benefits are obtained by using conventional divergence diffusion which has the following effects:-

(i) Improves the fit of the assimilation to the observed data.

(ii) Reduces "noise" in the assimilation.

(iii) Improves significantly the smoothness and fit to data of the tropical wind fields.

(iv) Improves the fit data of the subsequent 24 hour forecast.

Undesirable side effects of the method were not found to be significant in these runs.

ERENCES

ASSELIN, R. (1972) Frequency filter for time integrations. Mon. Wea. Rev., 100, 487-490.

BOURKE, W. (1974) A multi-level spectral model. I. Formulation and hemispheric integration. Mon. Wea. Rev., 102, 687-701.

DEY, C.H. (1978) Noise supression in a primitive equation prediction model. Mon. Wea. Rev., 106, 159-173.

LYNE, W.H. (1979) Data assimilation by repeated correction of model fields - theoretical considerations. Met O 11 Tech. Note. No. 130.

SHUMAN, F.G. and STACKPOLE, J.D. (1969) The currently operational NMC model and results from a recent numerical experiment. Proc. WMO/IUGG Symp. on Numerical Weather Prediction, Tokyo, Japan Meteor. Agency, II, 85-98.

TEMPERTON, C. and WILLIAMSON, D.L. (1979) Normal mode initialisation for a multi-level grid point model. ECMWF Tech. Report No. 11.

FIGURES

Figure 1 — Generation of gravity wave by insertion of data

Horizontal lines represent pressure surfaces.

(i) A temperature observation which is colder than the model temperature field is marked by the cross.

(ii) Insertion of the data results in the bending of the pressure surfaces in order to decrease thicknesses.

(iii) A horizontal pressure gradient exists now at P.

In the absence of damping effects or the modification of other variables outflow from the region will be produced in the next timestep of the integration. This will cause a raising of heights at points like Q and R . A repetition of this process will result in the propagation of a wave-like perturbation in the height field.

Figure 2 — Schematic time series of during first 6 hours of forecast

p_t^o represents a good observation. The mean value of the oscillation of the model p_* is consistent with p_t^o , but after six hours a difference ($p_t^M - p_t^o$) exists. If this difference is sufficiently large, p_t^o may be spuriously flagged by the Mode 1 check.

Figure 3 — Full update $g = 9.81\ ms^{-2}$, $f = 10^{-4} s^{-1}$, $H = 5$ km, $N = 0.37 \times 10^{-3} s^{-1}$

A $\mu = 0$ B $\mu = 0.5 \times 10^6\ m^2 s^{-1}$ C $\mu = 0.5 \times 10^7\ m^2 s^{-1}$ D $\mu = 1.5 \times 10^7\ m^2 s^{-1}$.

Figure 4 — Wind update only. Parameters and labelling as Fig 3.

Figure 5 — Height update only. Parameters and labelling as Fig 3.

Figure 6 — Regions of stable values for μ , taking $\Delta t = 300$S, $C = 311\ ms^{-1}$, d gridlength at 50N.

igure 7 Time series of surface pressure at 45N OE during assimilation. A control B enhanced diffusion C conventional divergence diffusion D enhanced integrated divergence damping E no divergence damping.

Figure 8 Time series of surface pressure during first 6 hours of forecast at 45N OE. A,B,C as Fig 7.

Figure 9 Time series of global RMS pressure tendency during assimilation. A,B,C as Fig. 7.

Figure 10 Time series of global RMS pressure tendency during first six hours of forecast. A, B, C as Fig. 7.

Figure 11 Times series of global RMS divergence during assimilation. A,B,C as Fig. 7.

Figure 12 Time series of global RMS divergence during first six hours of forecast. A,B,C as Fig. 7.

Figure 13 Time series of geopotential height during assimilation of sigma level 3 (≈ 0.935).
A control B conventional divergence diffusion.

Figure 14 Time series of geopotential height during assimilation of sigma level 5 (≈ 0.790). A, B as Fig. 13.

Figure 15 Time series of geopotential height during assimilation of sigma level 9 (≈ 0.390). A, B as Fig. 13.

Figure 16 MSLP chart from control run. Values and positions of certain features taken from the hand analysed chart are shown. Assimilation field.

Figure 17 As Fig. 16 but from run with conventional divergence diffusion.

Figure 18 250 mb wind field from control run produced by assimilation. Some areas of winds over 60 knots from the model marked by solid lines. Areas taken from the hand analysed marked by dashed lines. Spot values at numbered positions.

	Observed	Model
1	120	140
2	145	135
3	115	105
4	80	70
5	70	75

Figure 19 As Fig 18 but from run with conventional divergence diffusion. Spot values.

	Observed	Model
1	120	130
2	145	135
3	115	105
4	80	70
5	70	70

Figure 20 250 mb wind field from 45N-45S from control run. Africa and South America. From assimilation.

Figure 21 As Fig. 20 but using conventional divergence diffusion.

Figure 22 As Fig. 20 but covering Asia and Australia.

Figure 23 As Fig. 22 but using conventional divergence diffusion.

Figure 24 As Fig. 20 but covering the Pacific.

Figure 25 As Fig. 24 but using conventional divergence diffusion.

Figure 26(i),(ii),(iii) 250 mb wind observations.

Figure 27 Zonal wind component at 60N, 13W-0W produced by assimilation. A control B enhanced diffusion C conventional divergence diffusion D Optimum interpolation.

Figure 28 Global mean dynamic rain accumulation during assimilation. A control B conventional divergence diffusion.

Figure 29 Global mean convective rain accumulation during assimilation. A,B as Fig. 28.

Figure 30 Arakawa 'B' grid as used in the assimilation model.

β^*, Θ, Γ points denoted by k and u, v points denoted by u, v .

FIG. 1

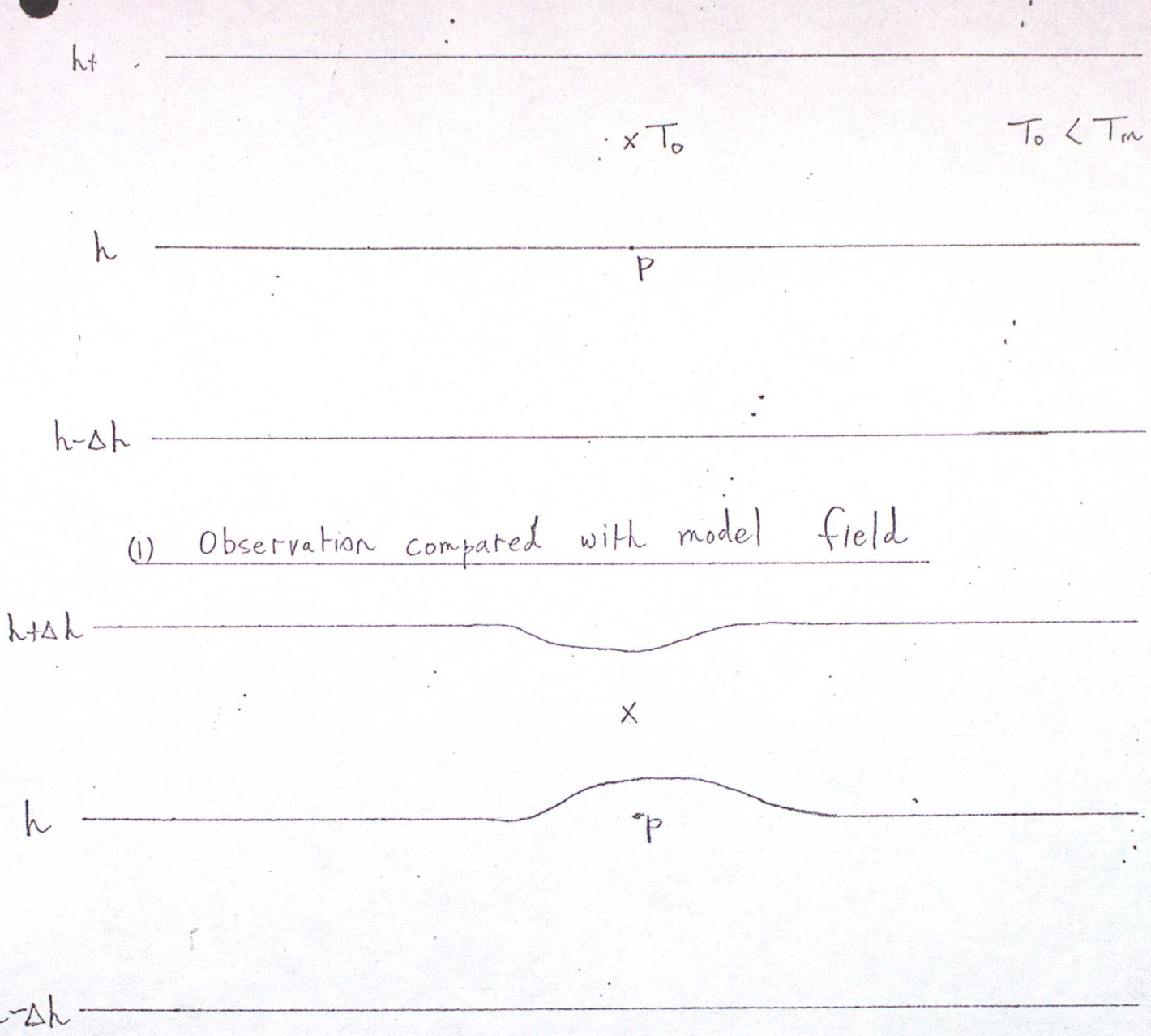

(i) Observation compared with model field

(ii) Insertion of data

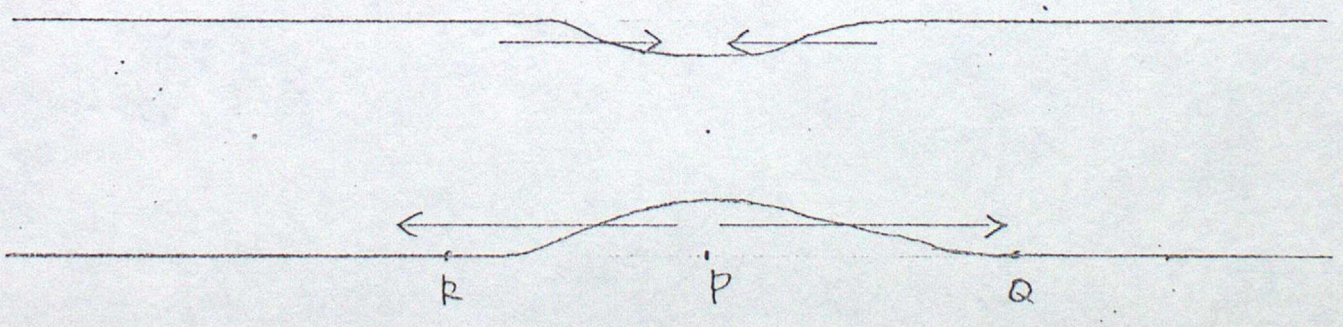

(iii) Next timestep of assimilation

FIG. 2

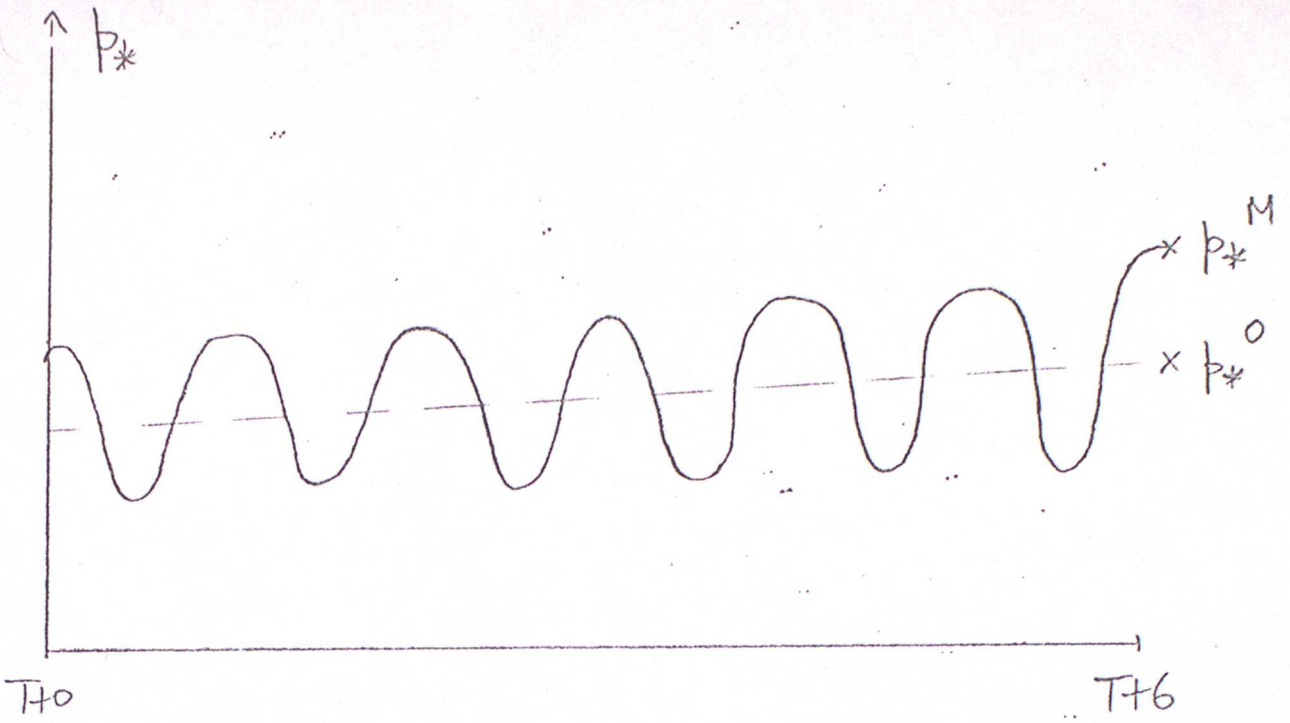

p_*^M – Model surface pressure

p_*^o – Observation surface pressure

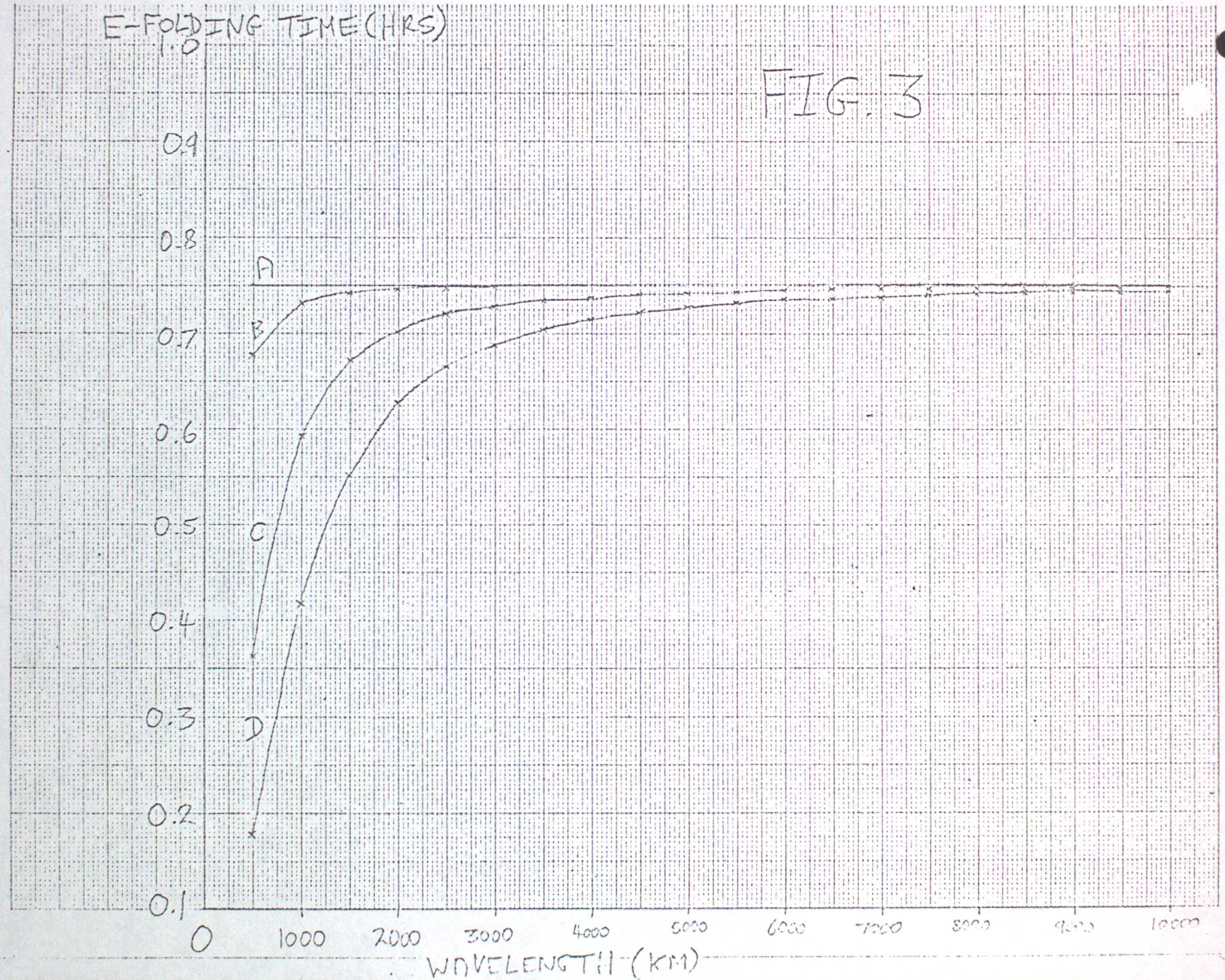
E-FOLDING TIME (HRS)
1.0
0.9
0.8
0.7
0.6
0.5
0.4
0.3
0.2
0.1
A
B
C
D
0
1000
2000
3000
4000
5000
6000
7000
8000
9000
10000
WAVELENGTH (KM)

FIG. 3

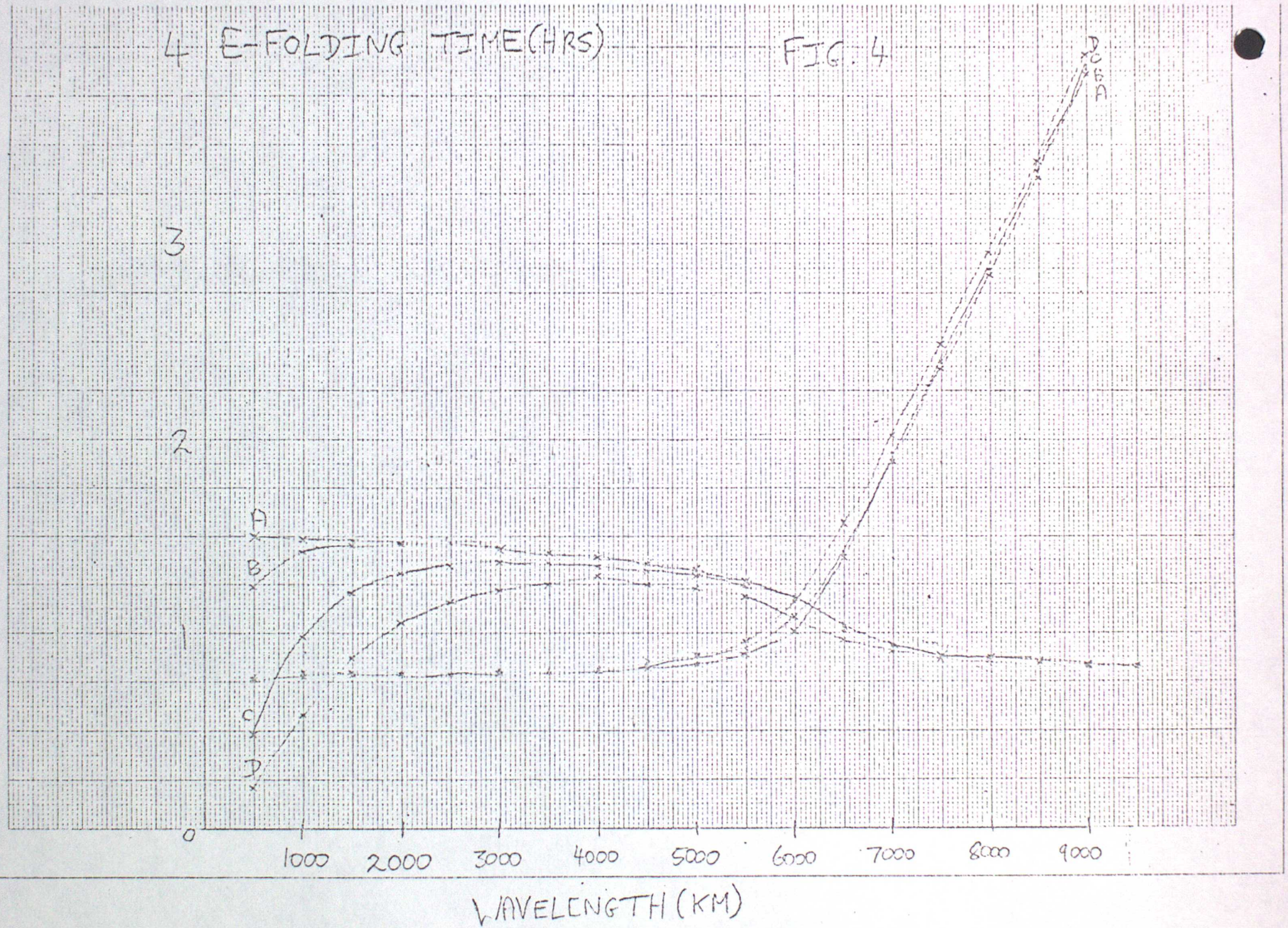
4
E-FOLDING TIME(HRS)
FIG. 4
3
2
1
0
A
B
C
D
D C B A
1000
2000
3000
4000
5000
6000
7000
8000
9000
WAVELENGTH (KM)

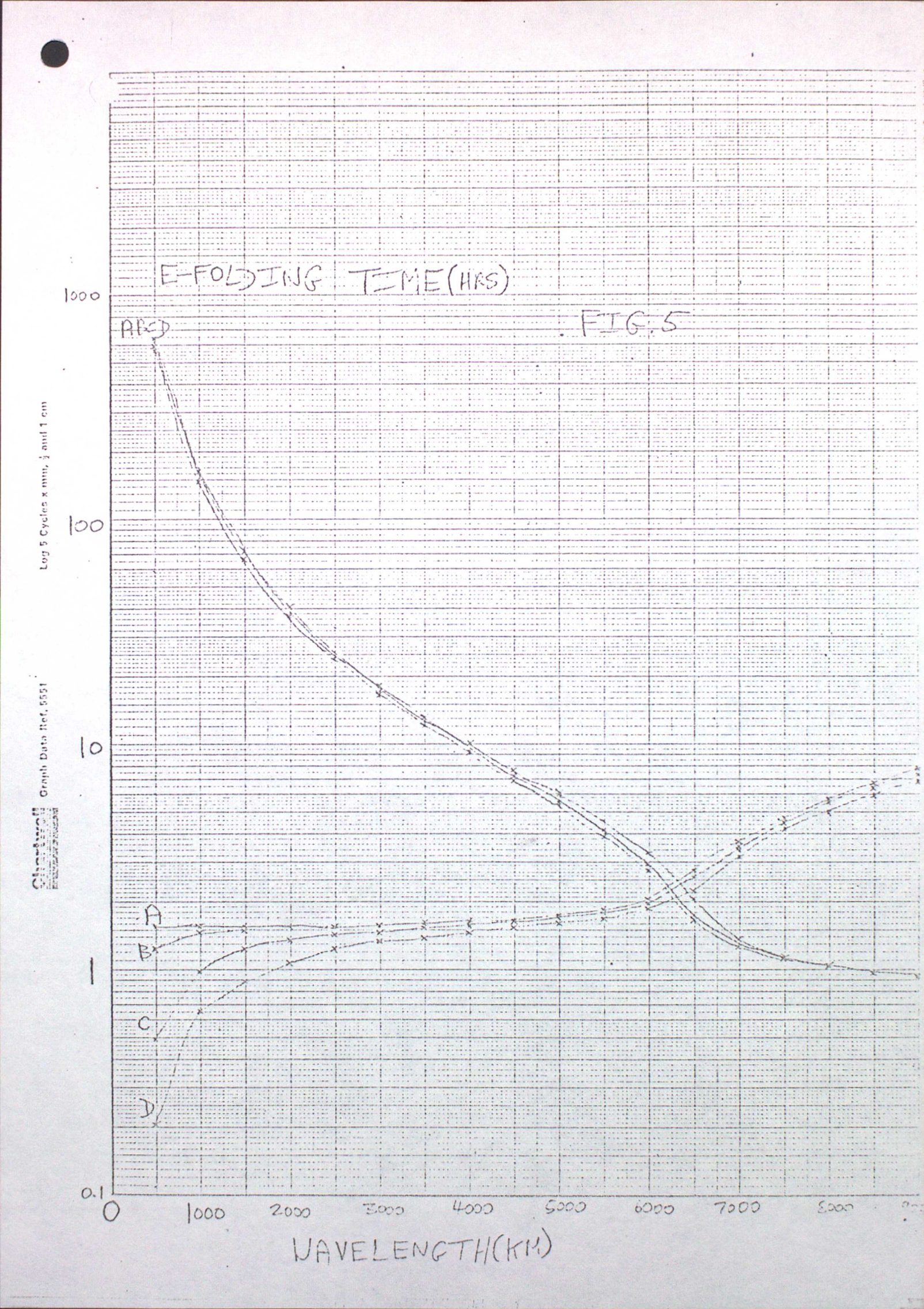
E-FOLDING TIME(HRS)
FIG. 5
1000
100
10
1
0.1
A&B
A
B
C
D
0
1000
2000
3000
4000
5000
6000
7000
8000
WAVELENGTH(KM)
Log 5 Cycles x mm, 2 and 1 cm
Graph Data Ref. 5551

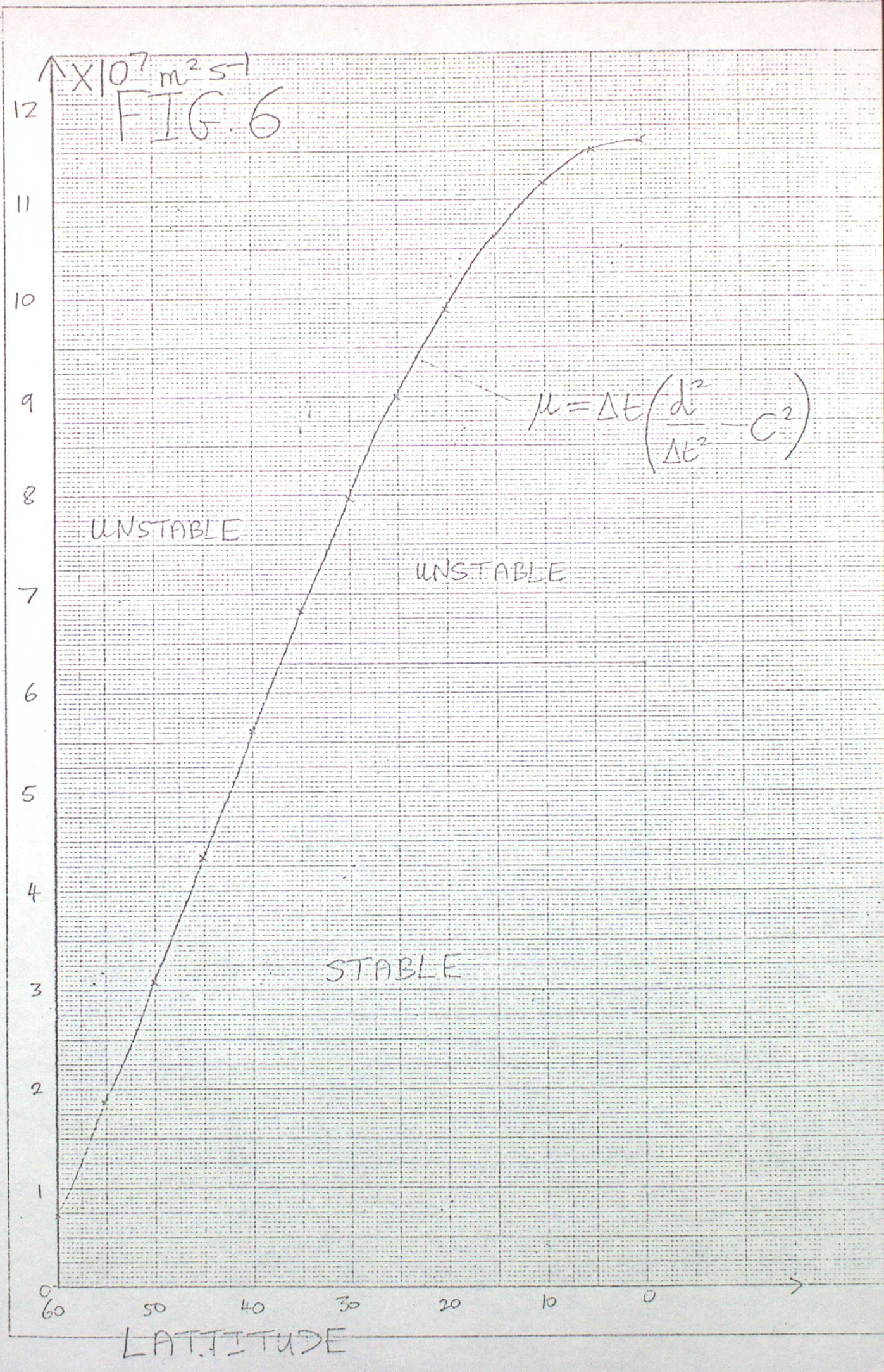
FIG. 6
$\times 10^7 \, m^2 s^{-1}$
12
11
10
9
8
7
6
5
4
3
2
1
0
$\mu = \Delta t \left(\frac{d^2}{\Delta t^2} - c^2 \right)$
UNSTABLE
UNSTABLE
STABLE
60
50
40
30
20
10
0
LATITUDE

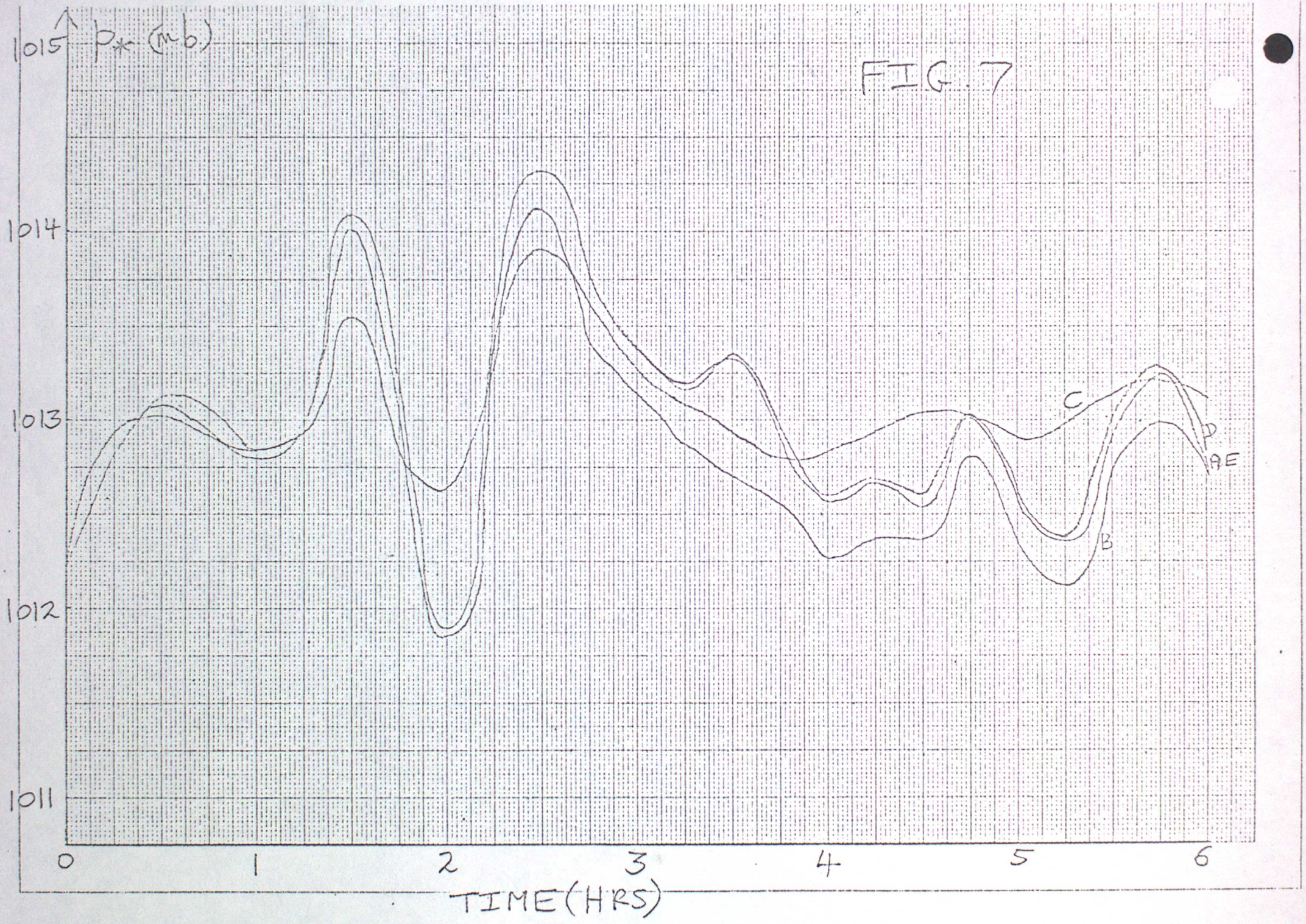
FIG. 7
1015
1014
1013
1012
1011
p* (mb)
0
1
2
3
4
5
6
TIME(HRS)
C
D
AE
B

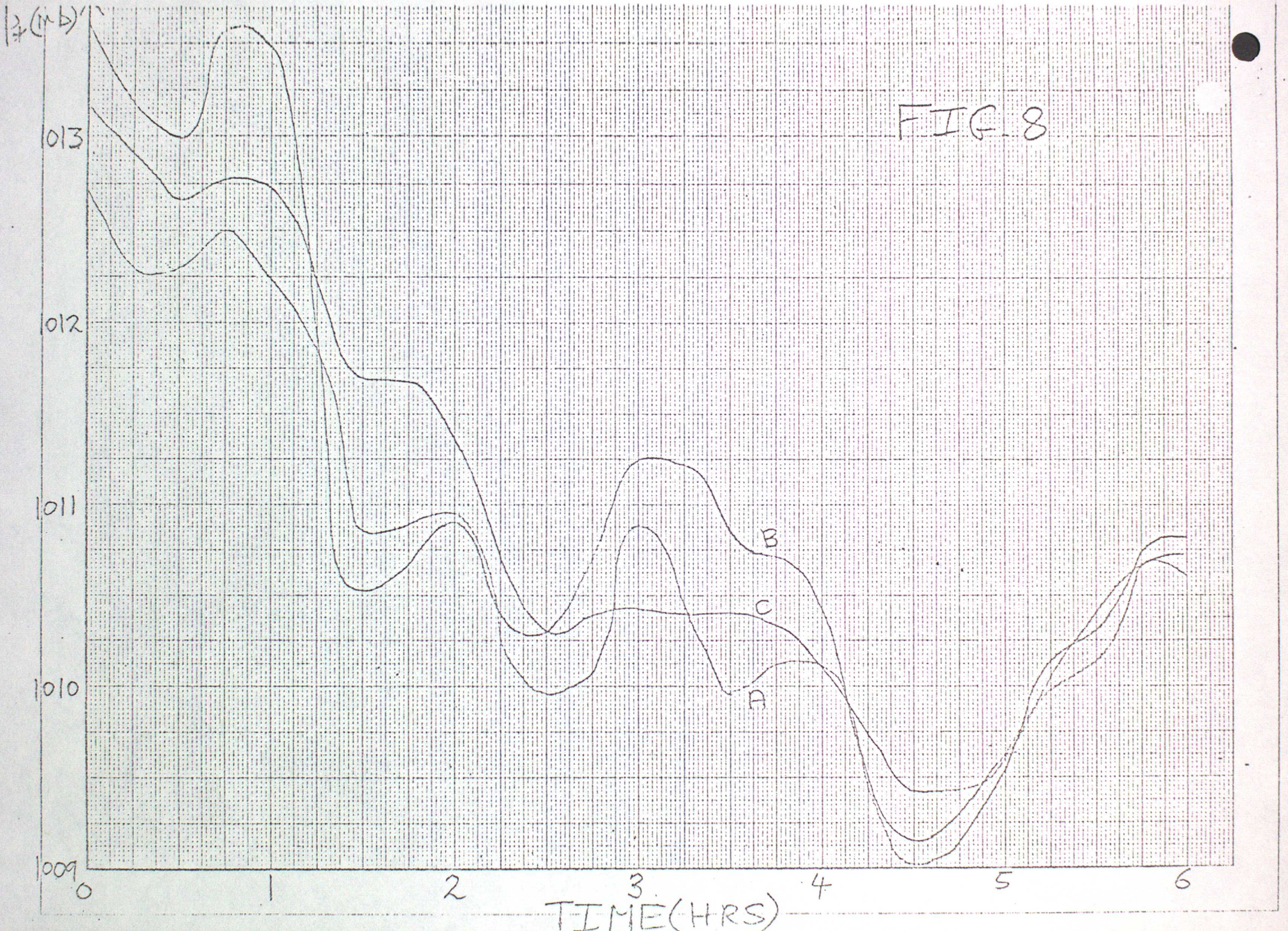
FIG. 8
P (mb)
1013
1012
1011
1010
1009
0
1
2
3
4
5
6
TIME (HRS)
A
B
C

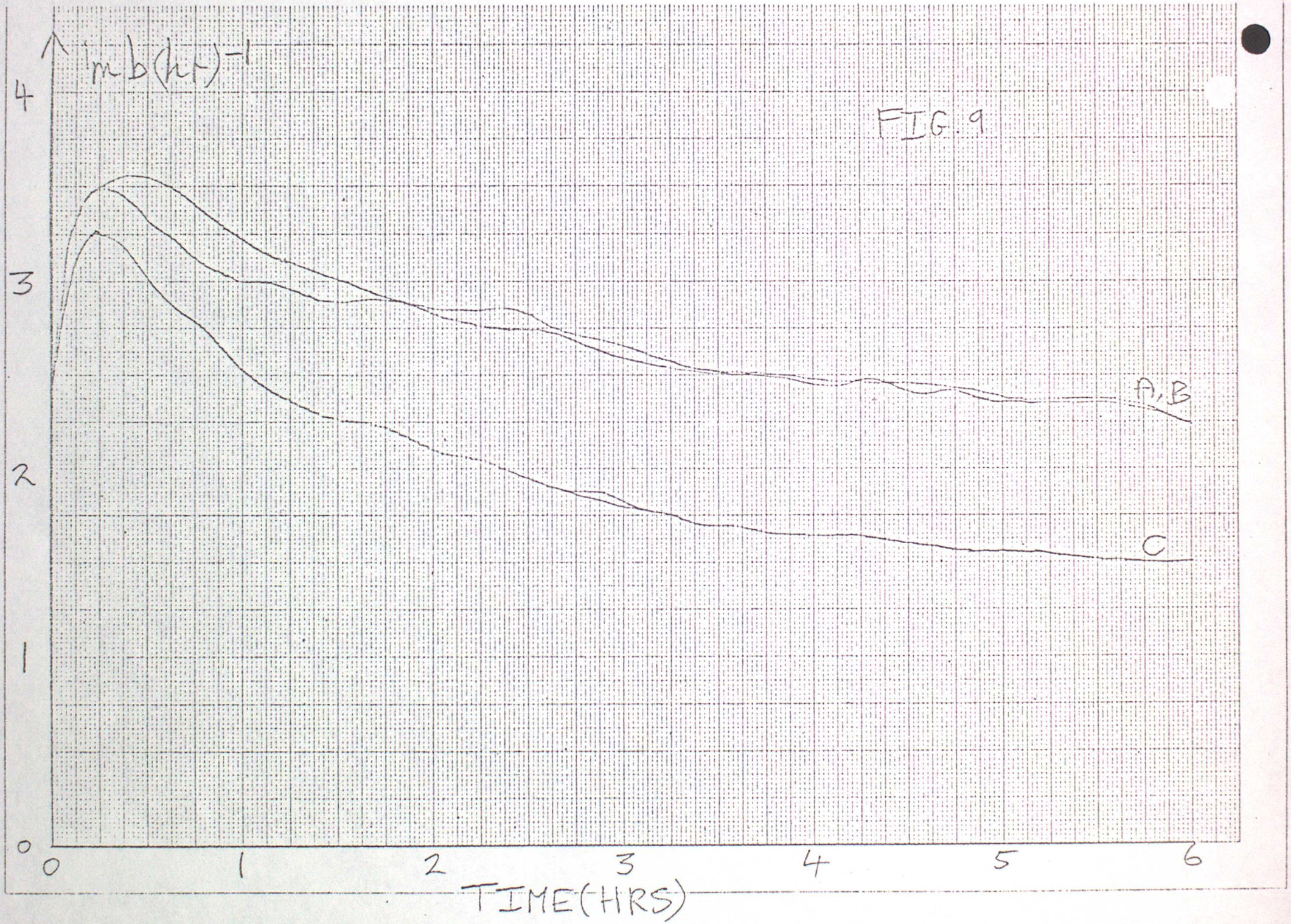
$[m-b(kt)^{-1}]$
FIG. 9
4
3
2
1
0
A, B
C
0
1
2
3
4
5
6
TIME (HRS)

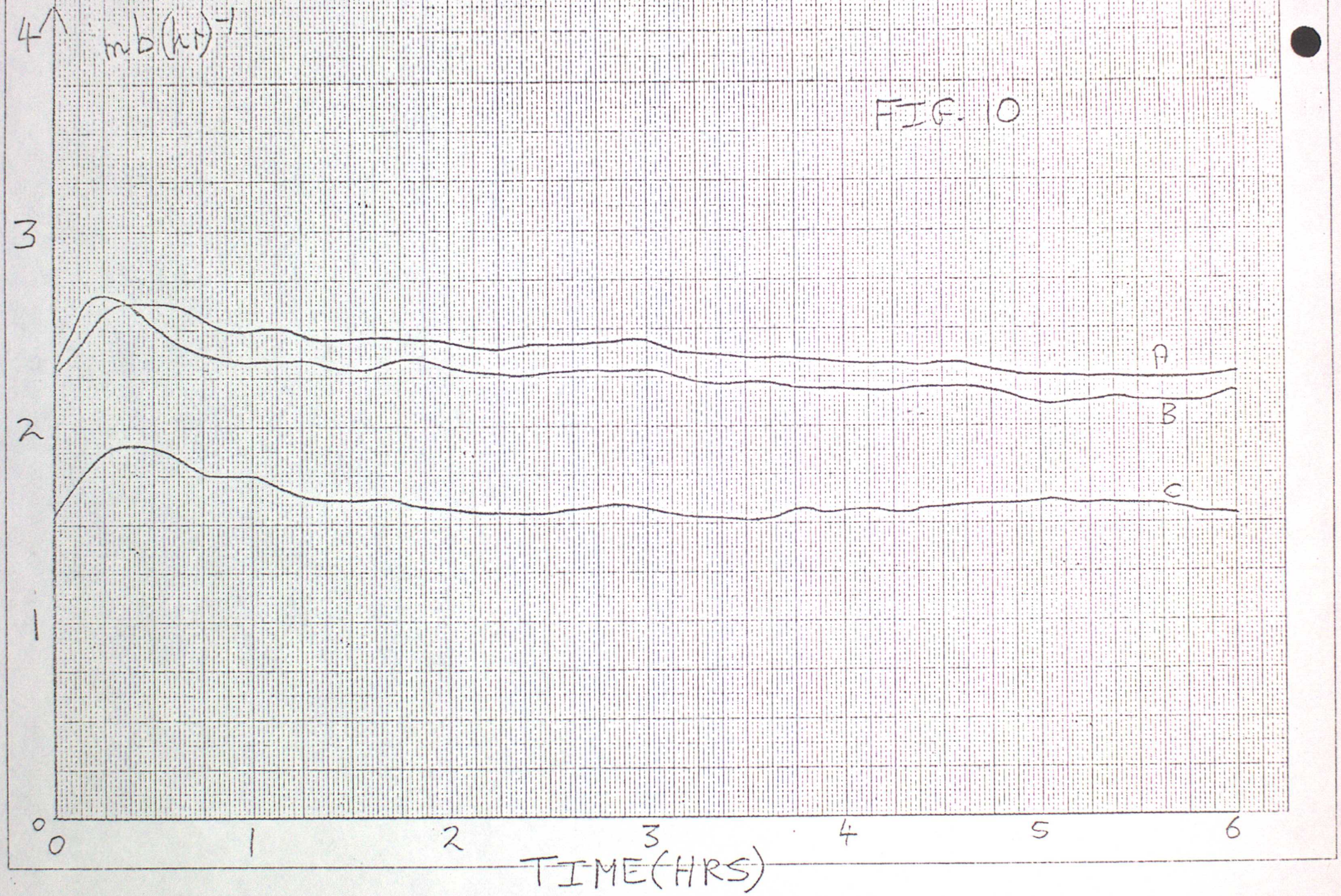
FIG. 10
4
3
2
1
0
mb(kt)⁻¹
0
1
2
3
4
5
6
TIME(HRS)
A
B
C

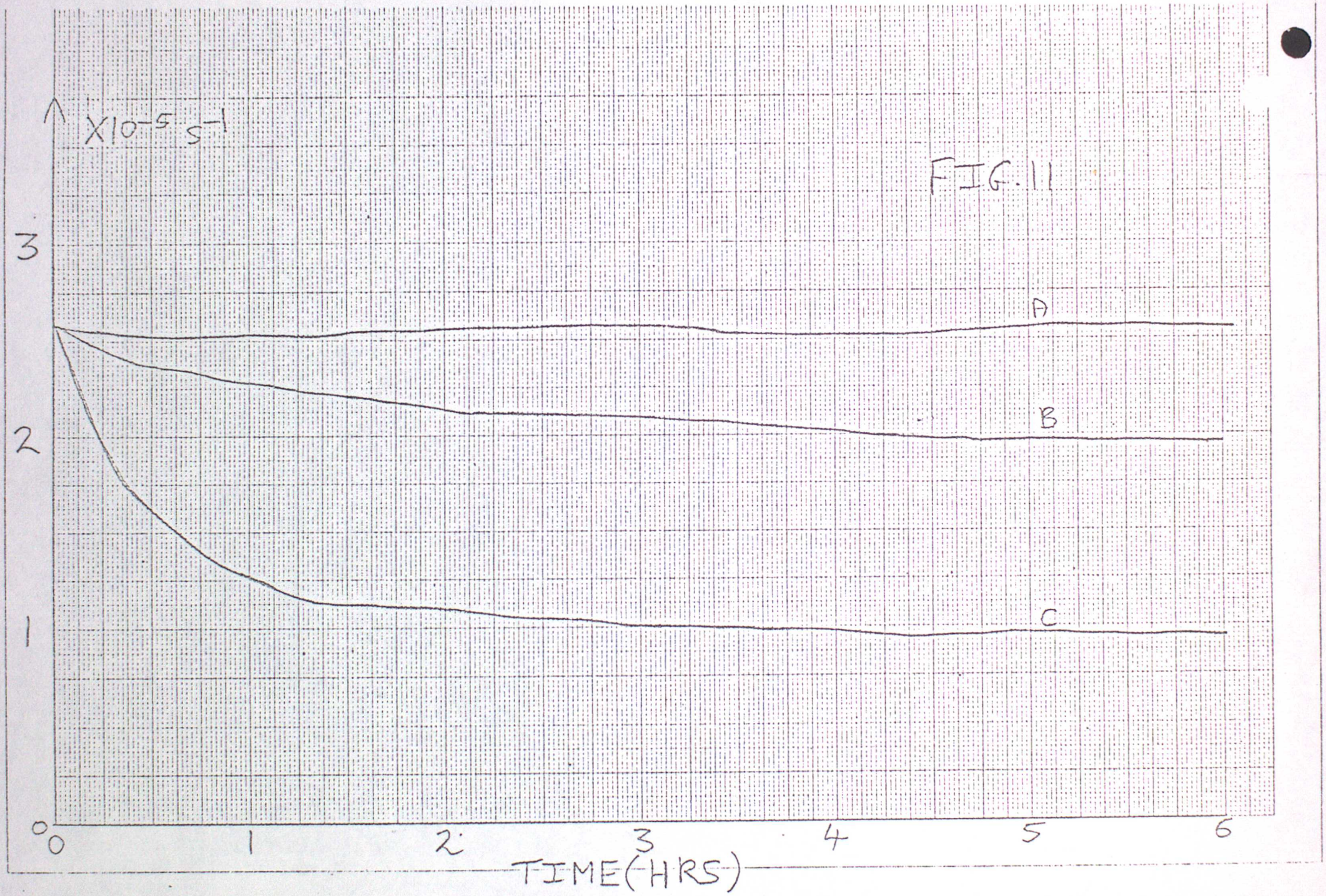
FIG. 11
X10⁻⁵ S⁻¹
3
2
1
0
A
B
C
0
1
2
3
4
5
6
TIME (HRS)

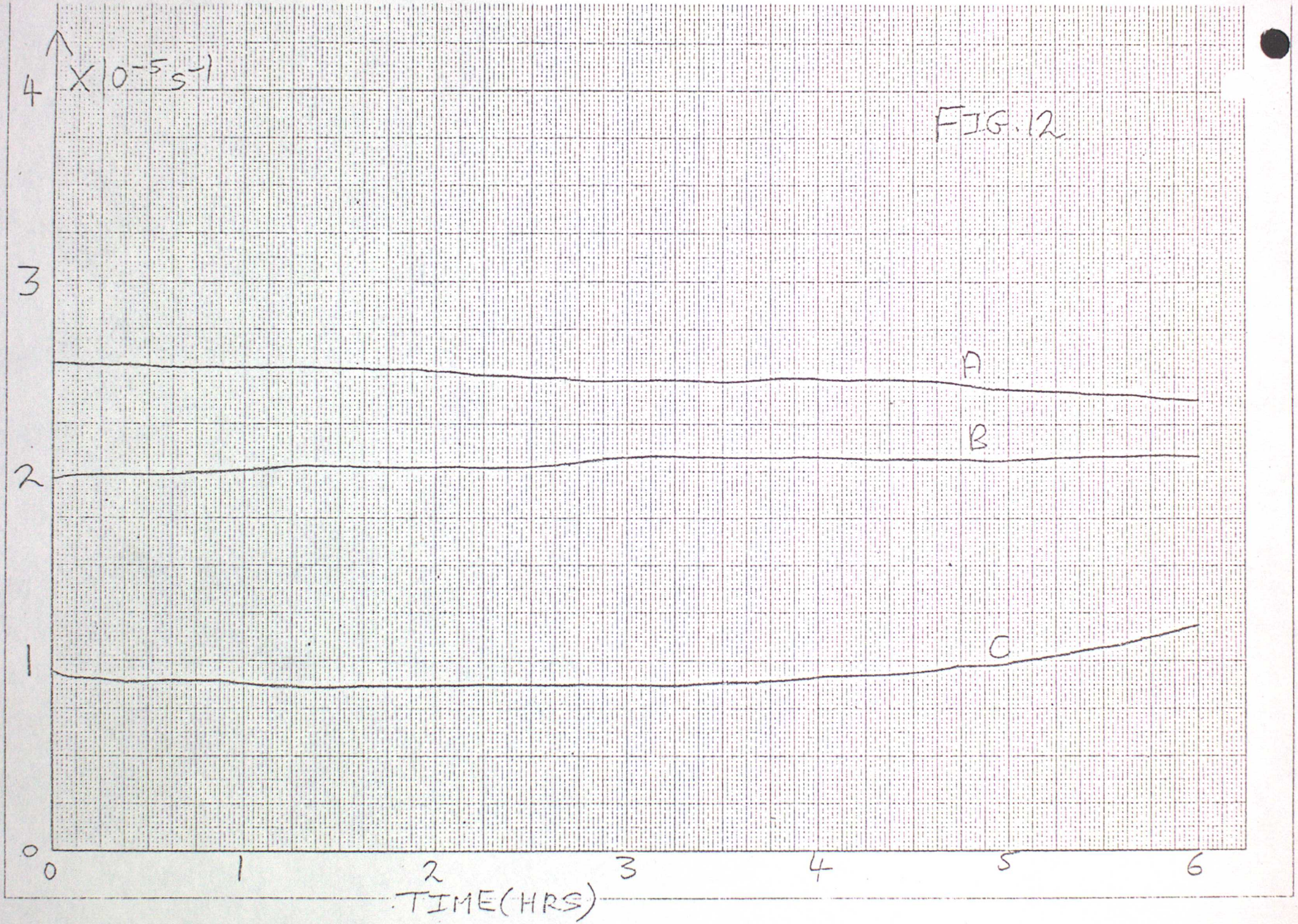
FIG. 12
X 10⁻⁵ s⁻¹
4
3
2
1
0
A
B
C
0
1
2
3
4
5
6
TIME (HRS)

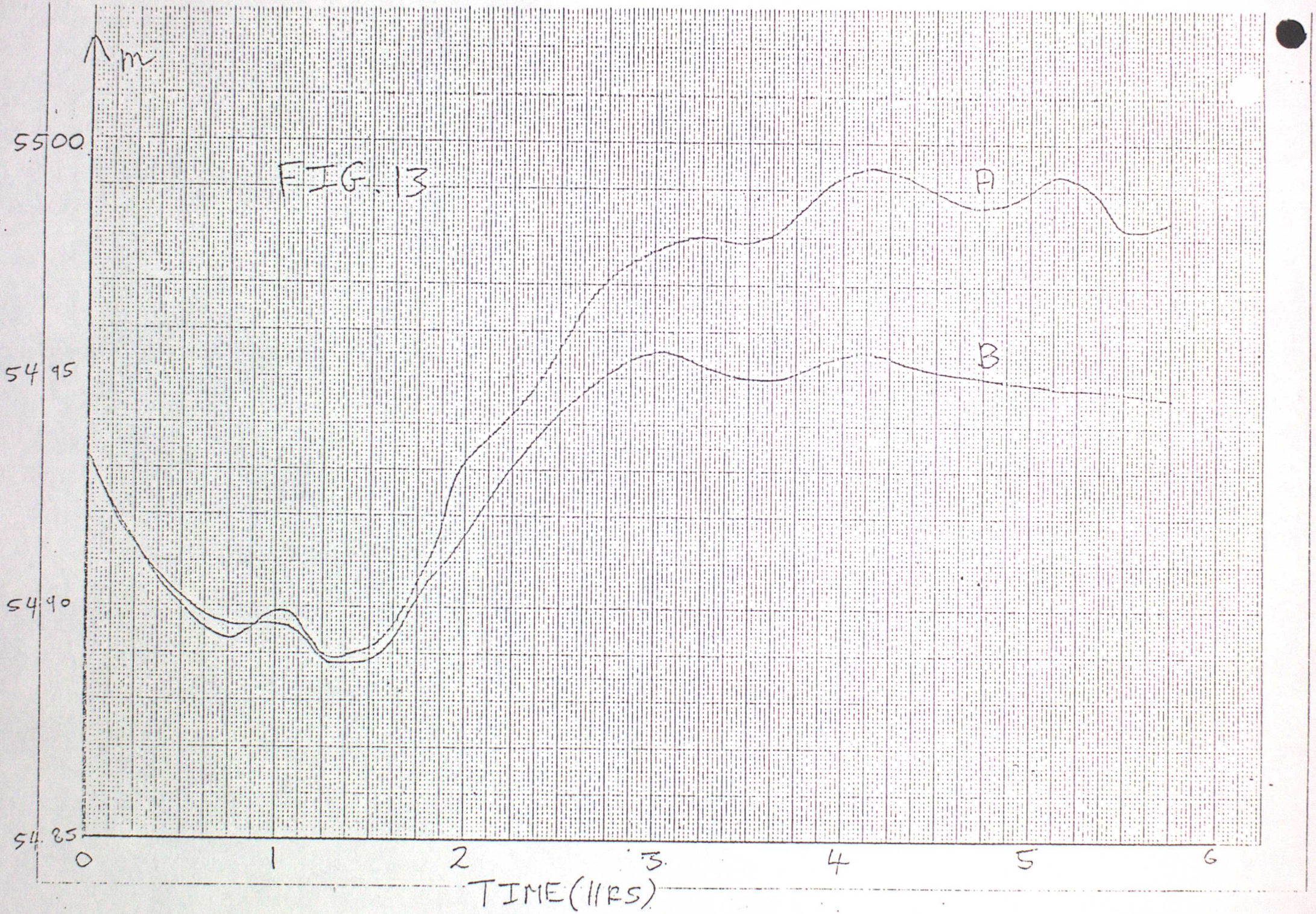
m
5500
5495
5490
5485
FIG. 13
A
B
0
1
2
3
4
5
6
TIME (HRS)

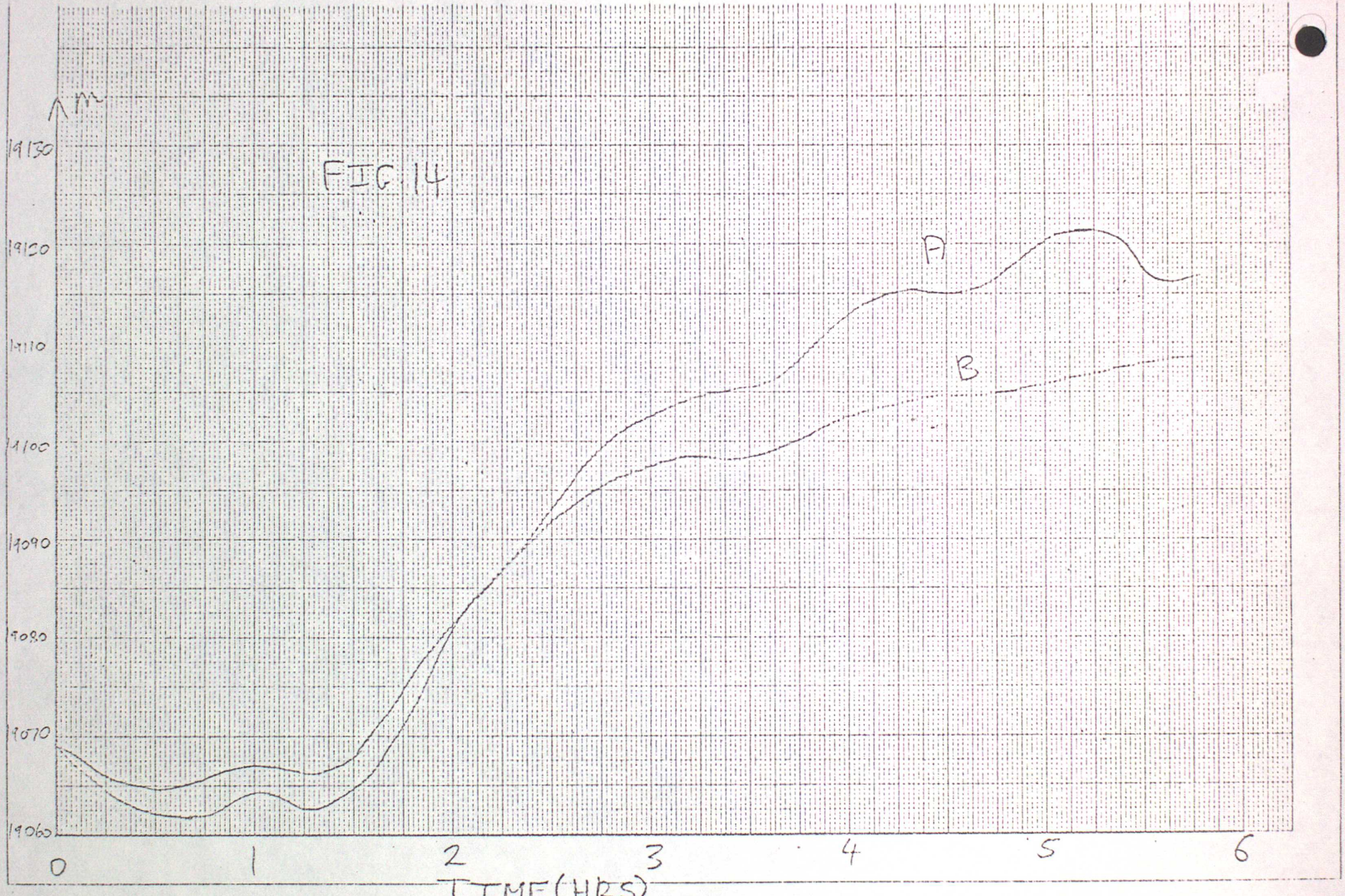
FIG 14
mm
19130
19120
19110
19100
19090
19080
19070
19060
A
B
0
1
2
3
4
5
6
TIME (HRS)

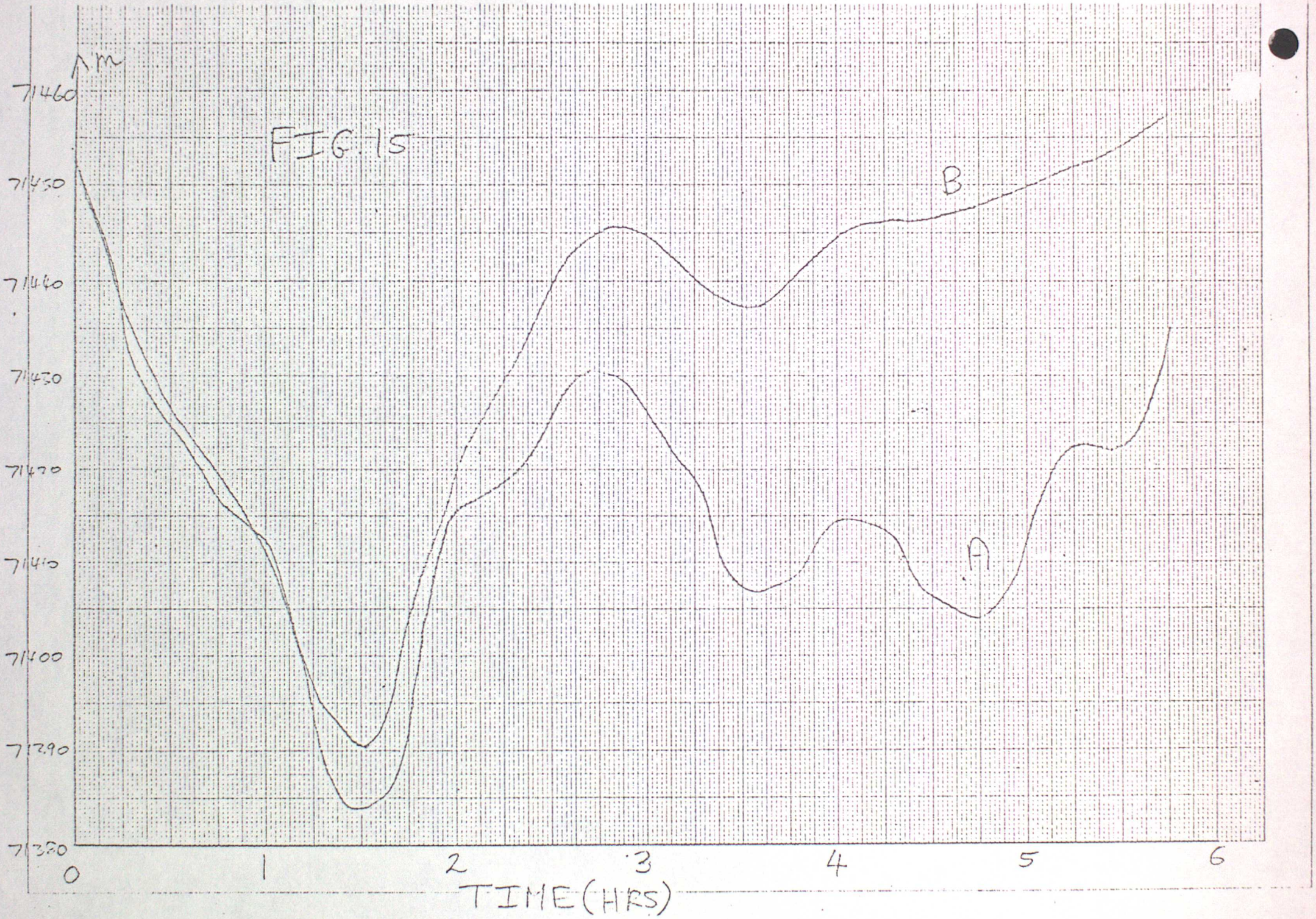
FIG. 15
m
71460
71450
71440
71430
71420
71410
71400
71390
71380
0
1
2
3
4
5
6
TIME (HRS)
B
A

FIG. 16

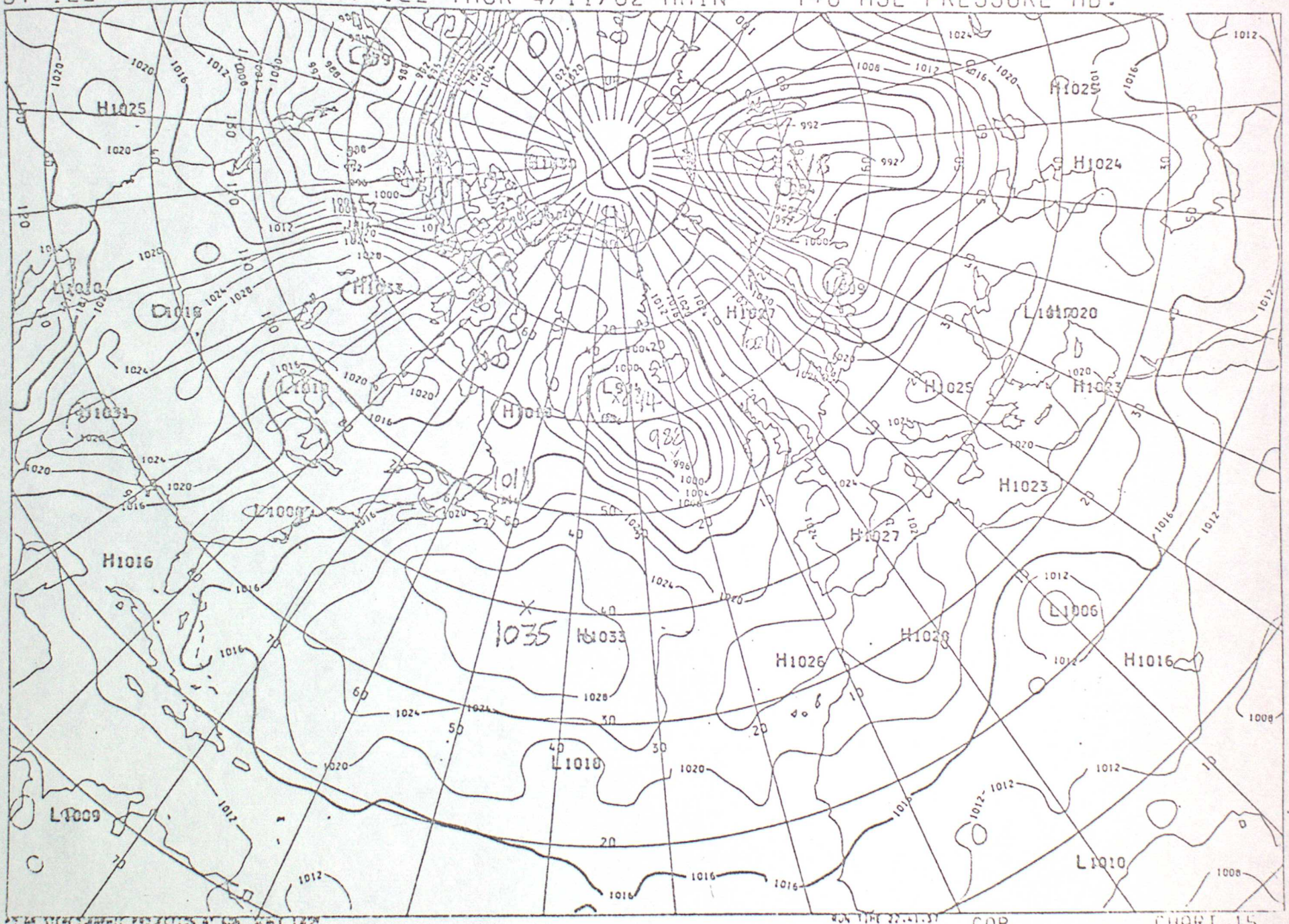
DT 12Z THUR 4/11/82 VT 12Z THUR 4/11/82 MAIN T+0 MSL PRESSURE MB.
H1025
H1024
H1023
H1027
H1033
H1031
H1016
H1026
H1028
L1020
L1006
L1010
L1009
1035
COP
CHART 15

IG.17

DT 12Z THUR 4/11/82 VT 12Z THUR 4/11/82 MAIN T+0 MSL PRESSURE MB.

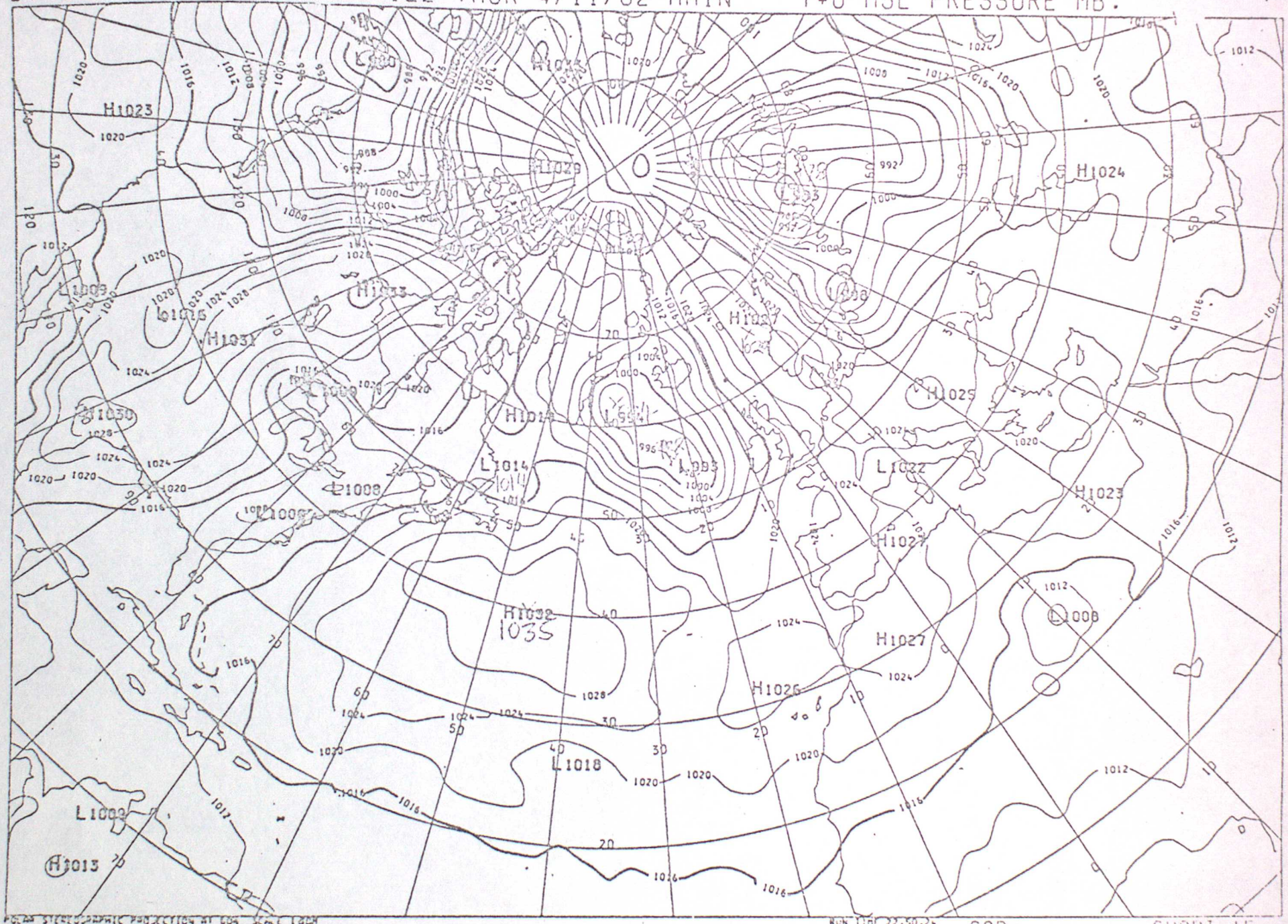

COP CHART 15

FIG.18

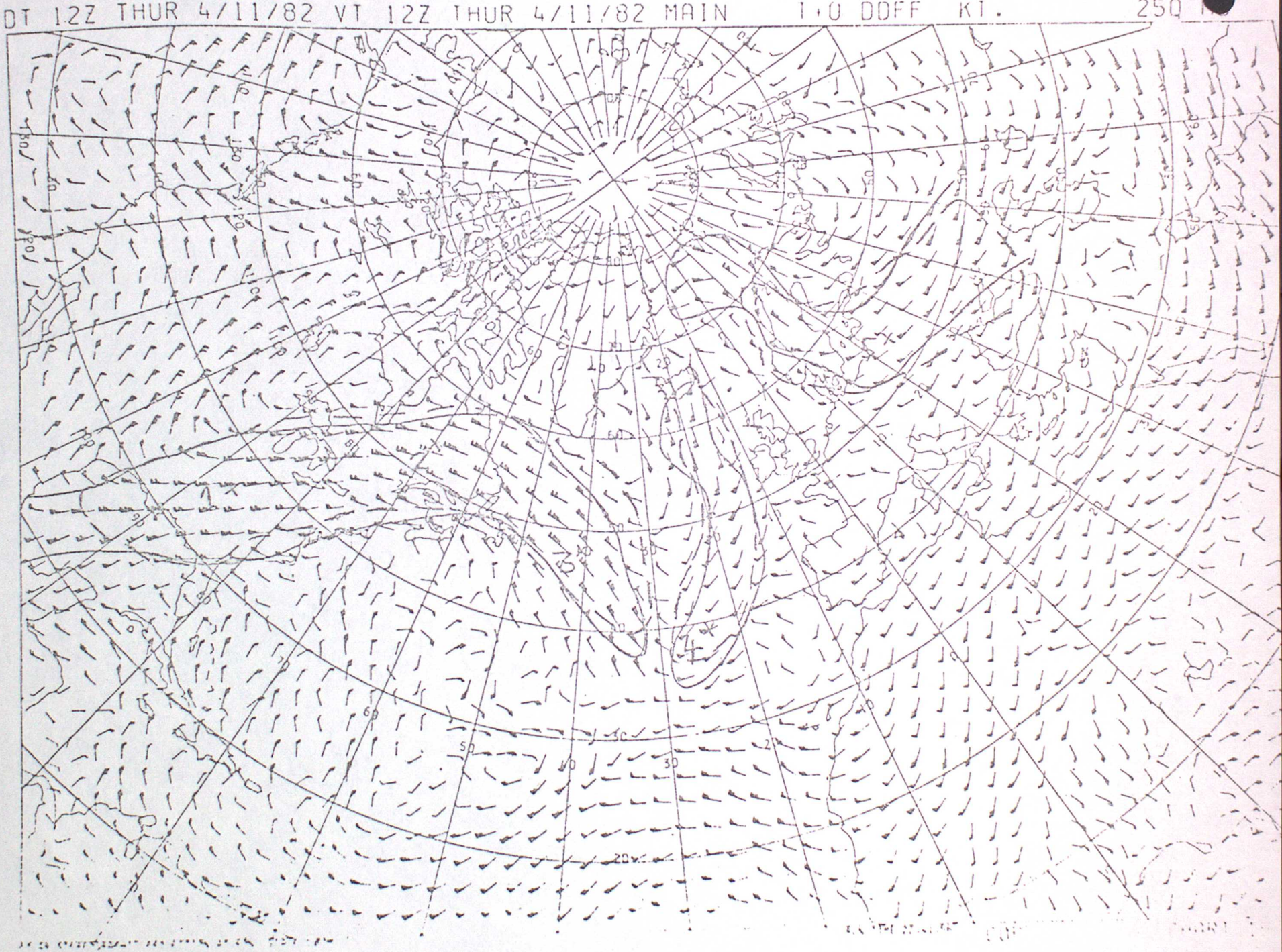

FIG. 19

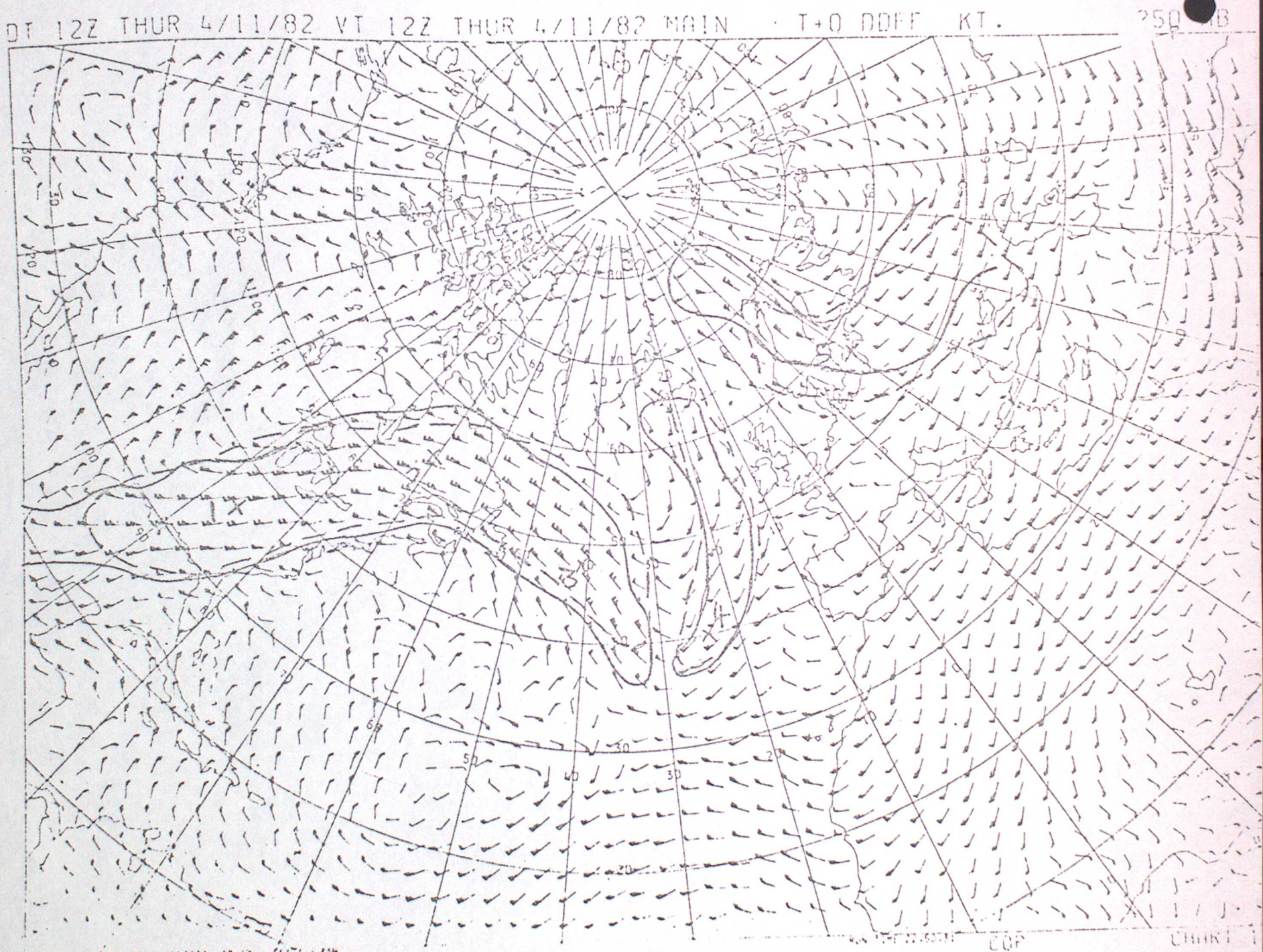

FIG.20

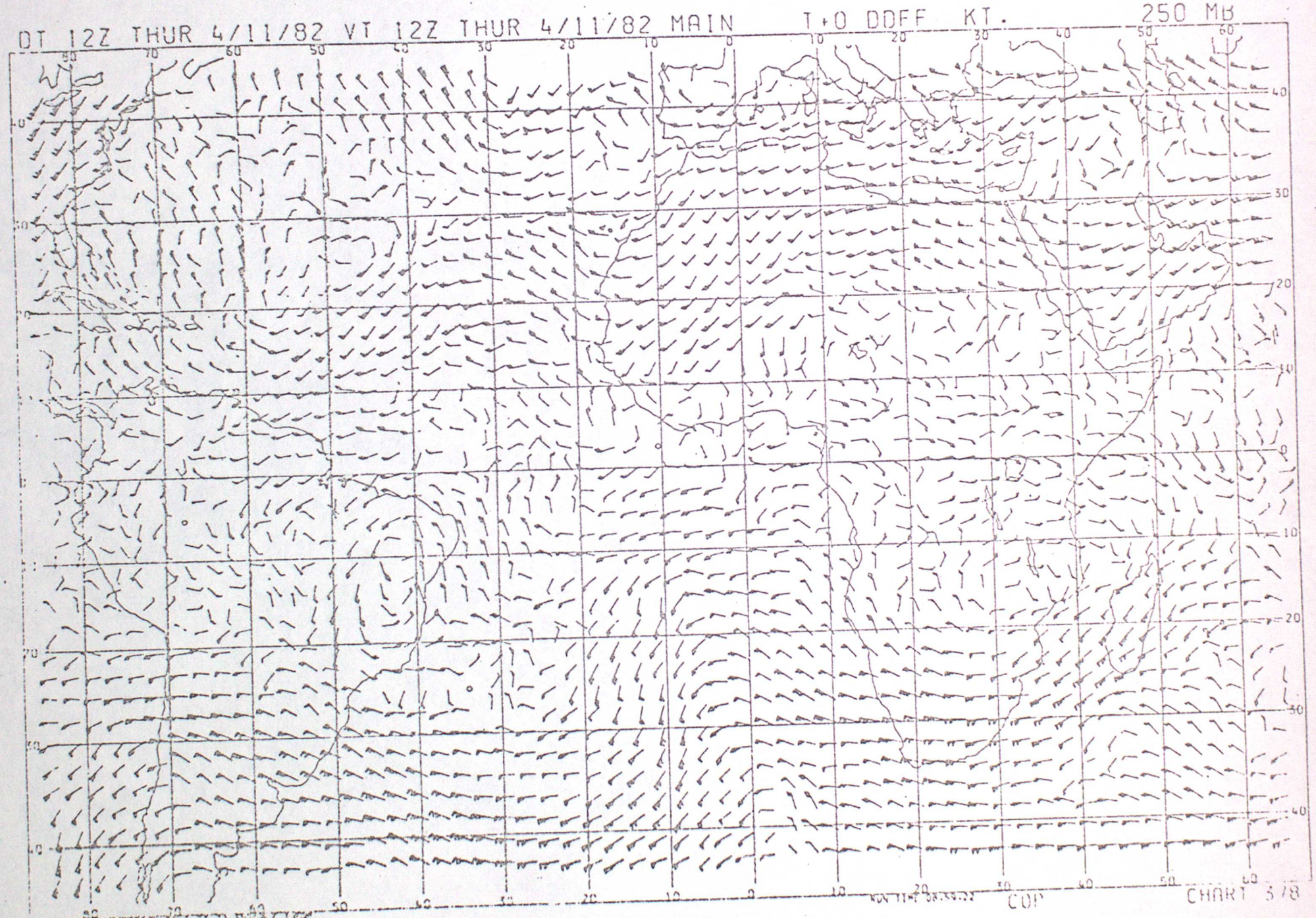
DT 12Z THUR 4/11/82 VT 12Z THUR 4/11/82 MAIN T+0 DOFF KT. 250 MB
COP
CHART 3/8

[FIG. 2]

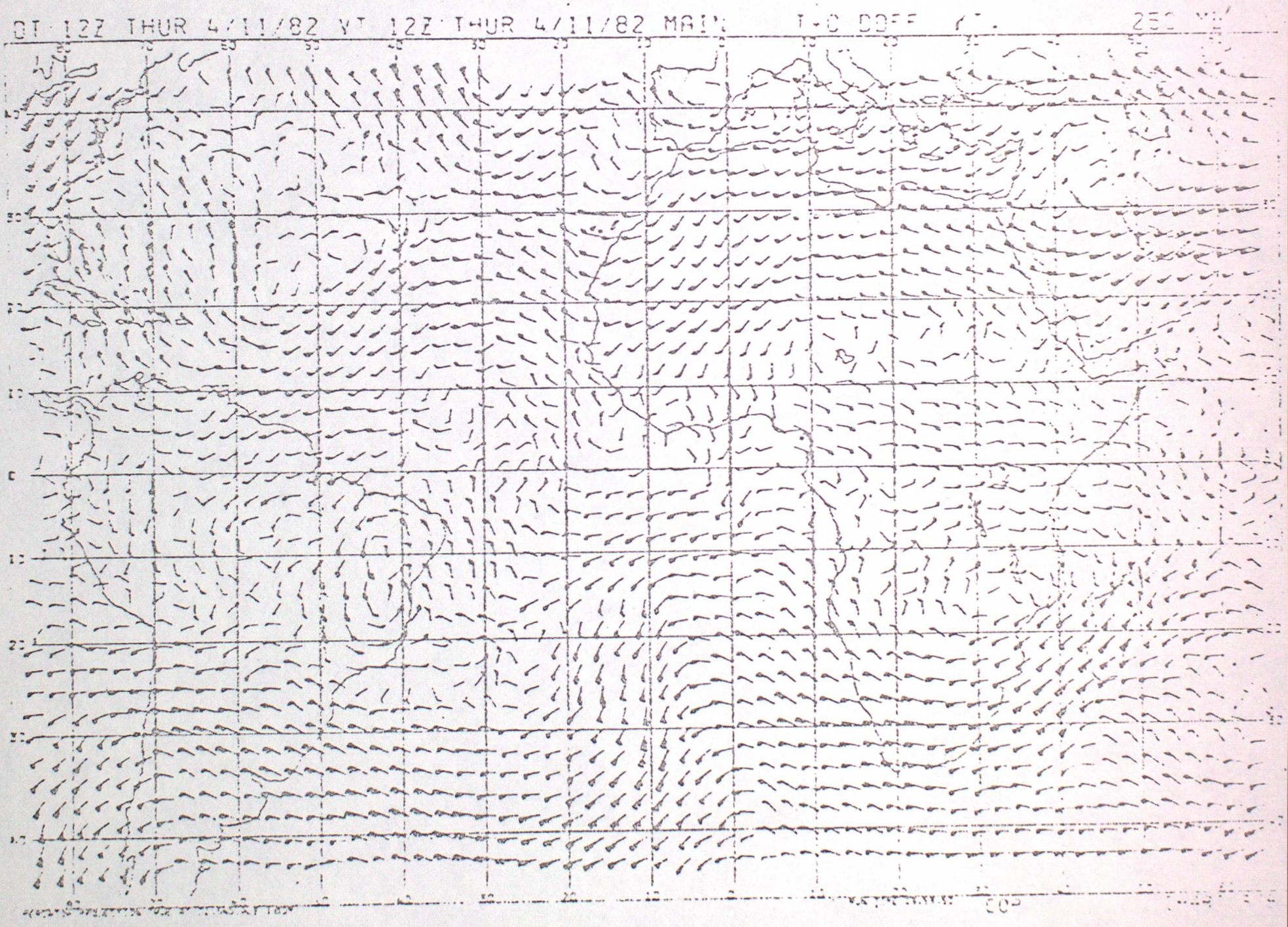

FIG. 22

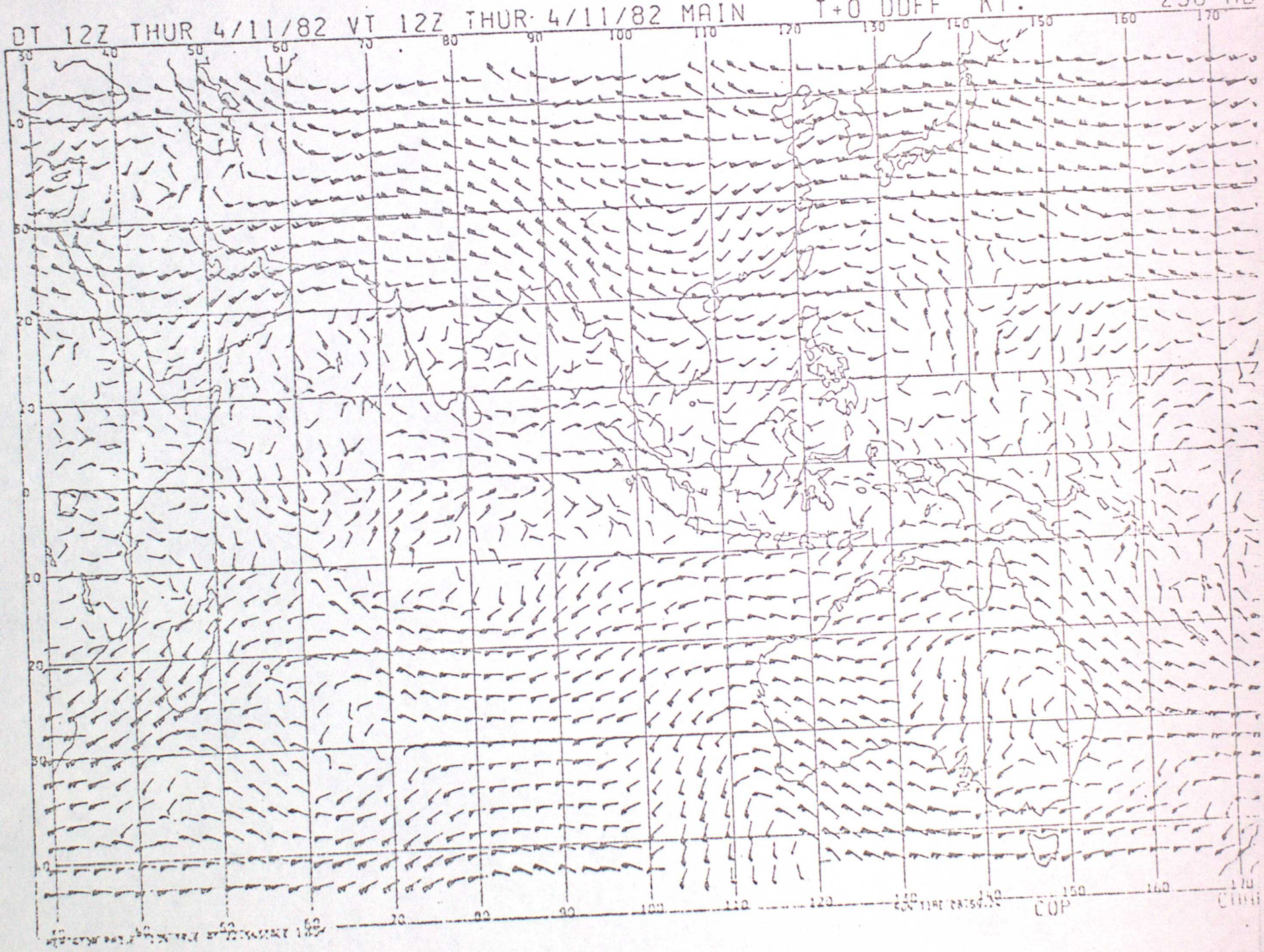

FIG.23

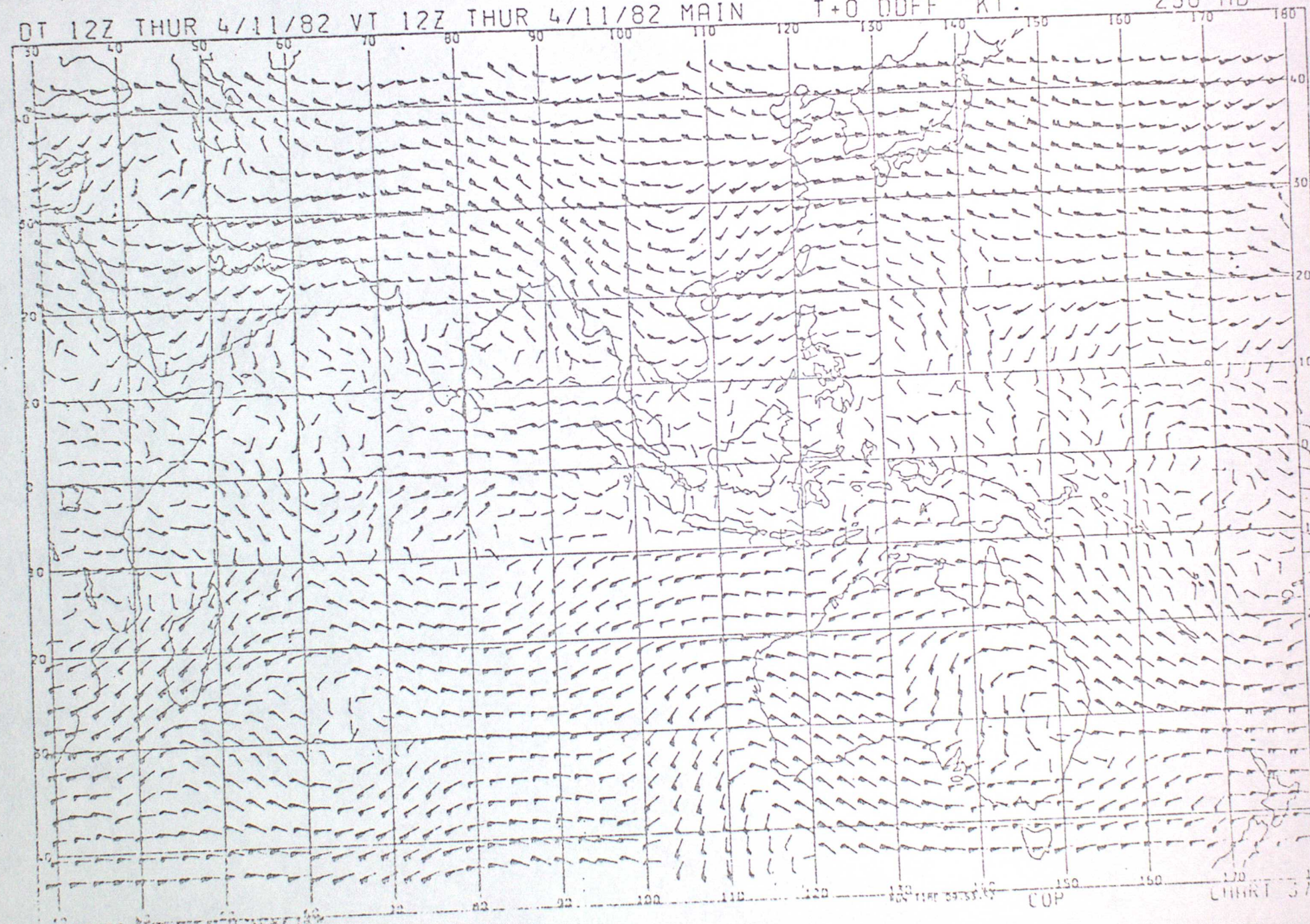
DT 12Z THUR 4/11/82 VT 12Z THUR 4/11/82 MAIN T+0 DDFF KT. 250 MB
CHART 37

FIG. 24

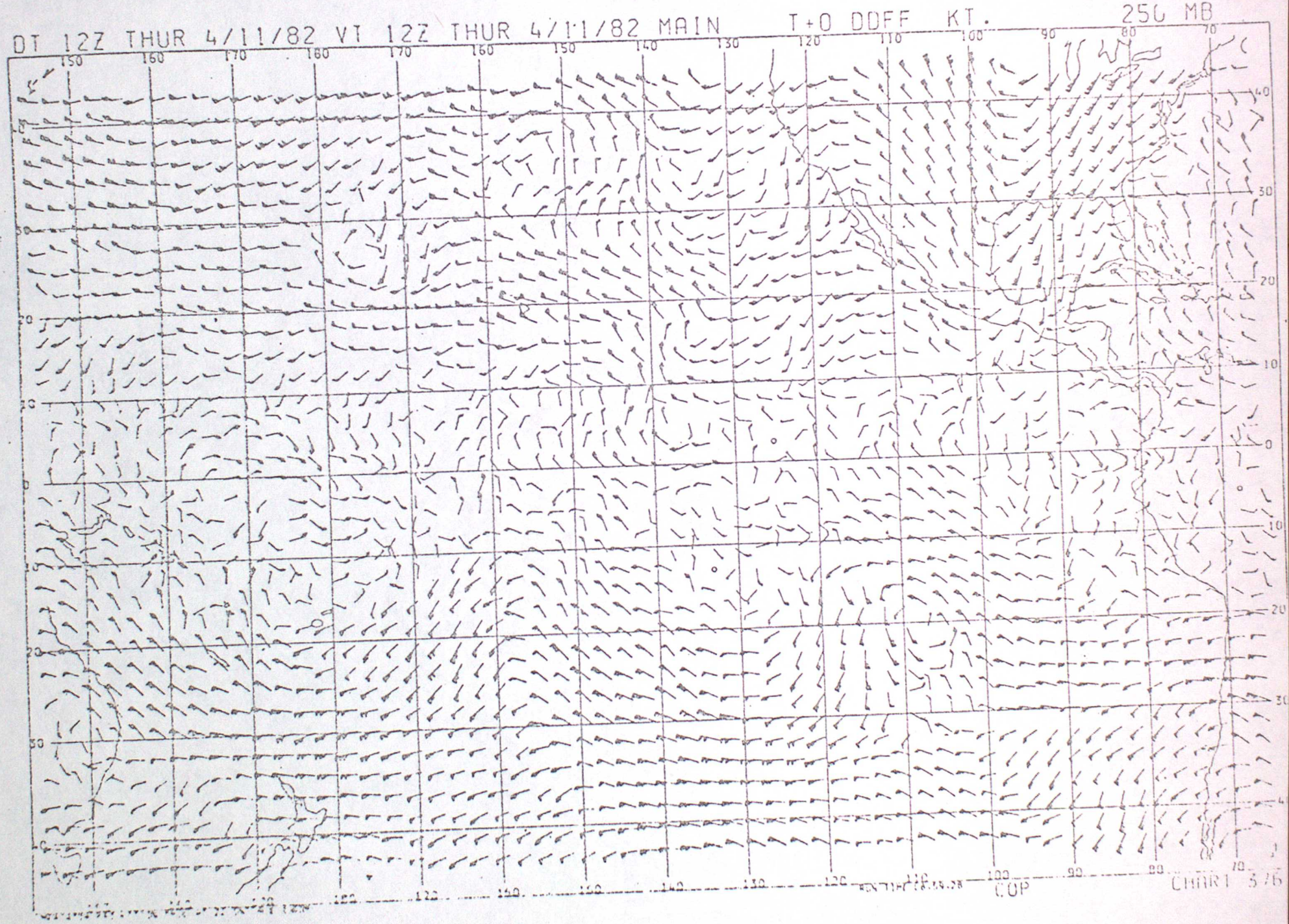
DT 12Z THUR 4/11/82 VT 12Z THUR 4/11/82 MAIN T+0 DDFF KT. 250 MB
COP
CHART 5/76

FIG. 25

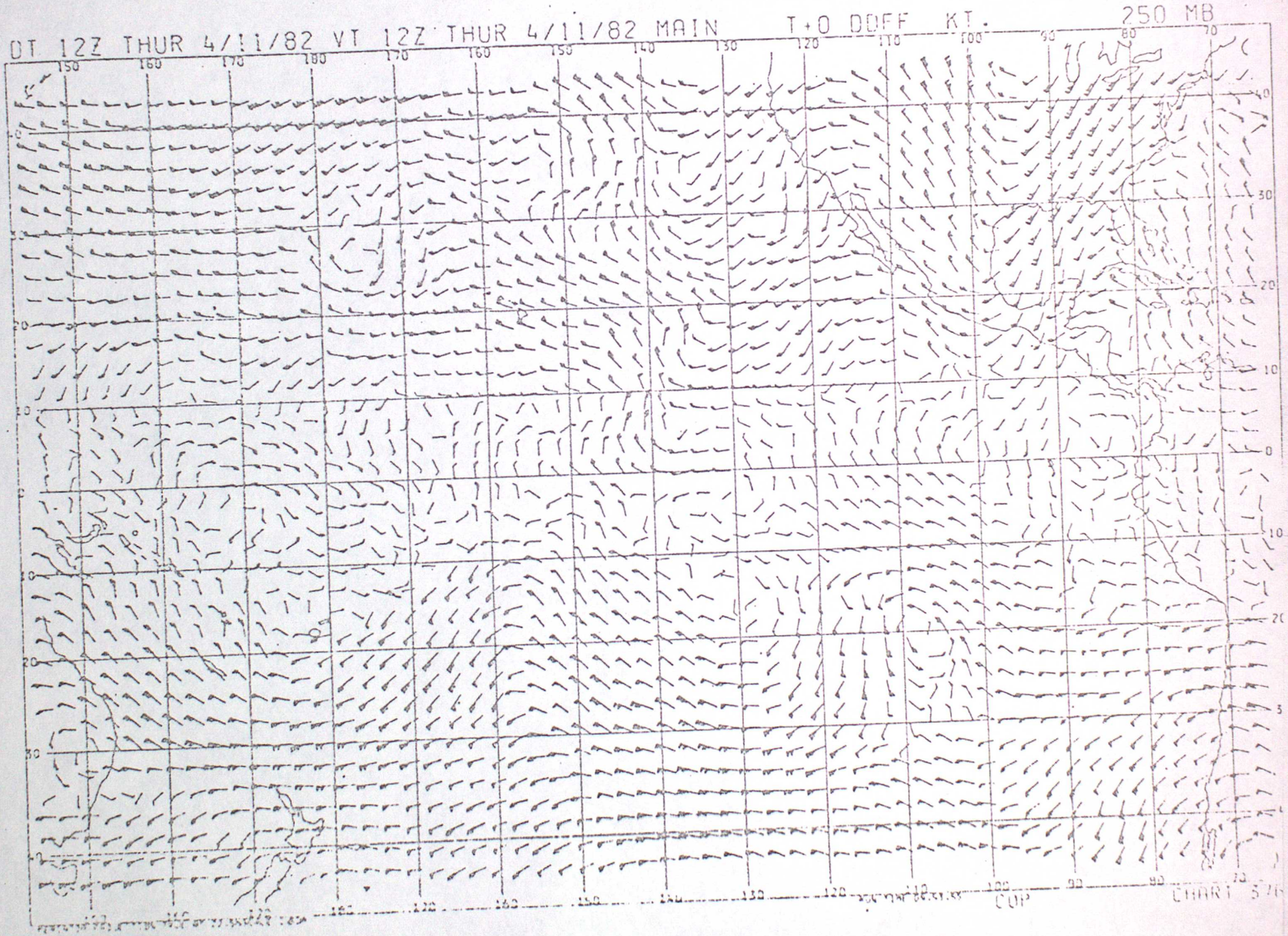
DT 12Z THUR 4/11/82 VT 12Z THUR 4/11/82 MAIN T+0 DOFF KT. 250 MB
CHART 5

FIG-26(i)

250 MB ON 4 NOV 1982 AT 12Z

MERCATOR PROJECTION SCALE 1:[illegible] AT 20.5° N/S

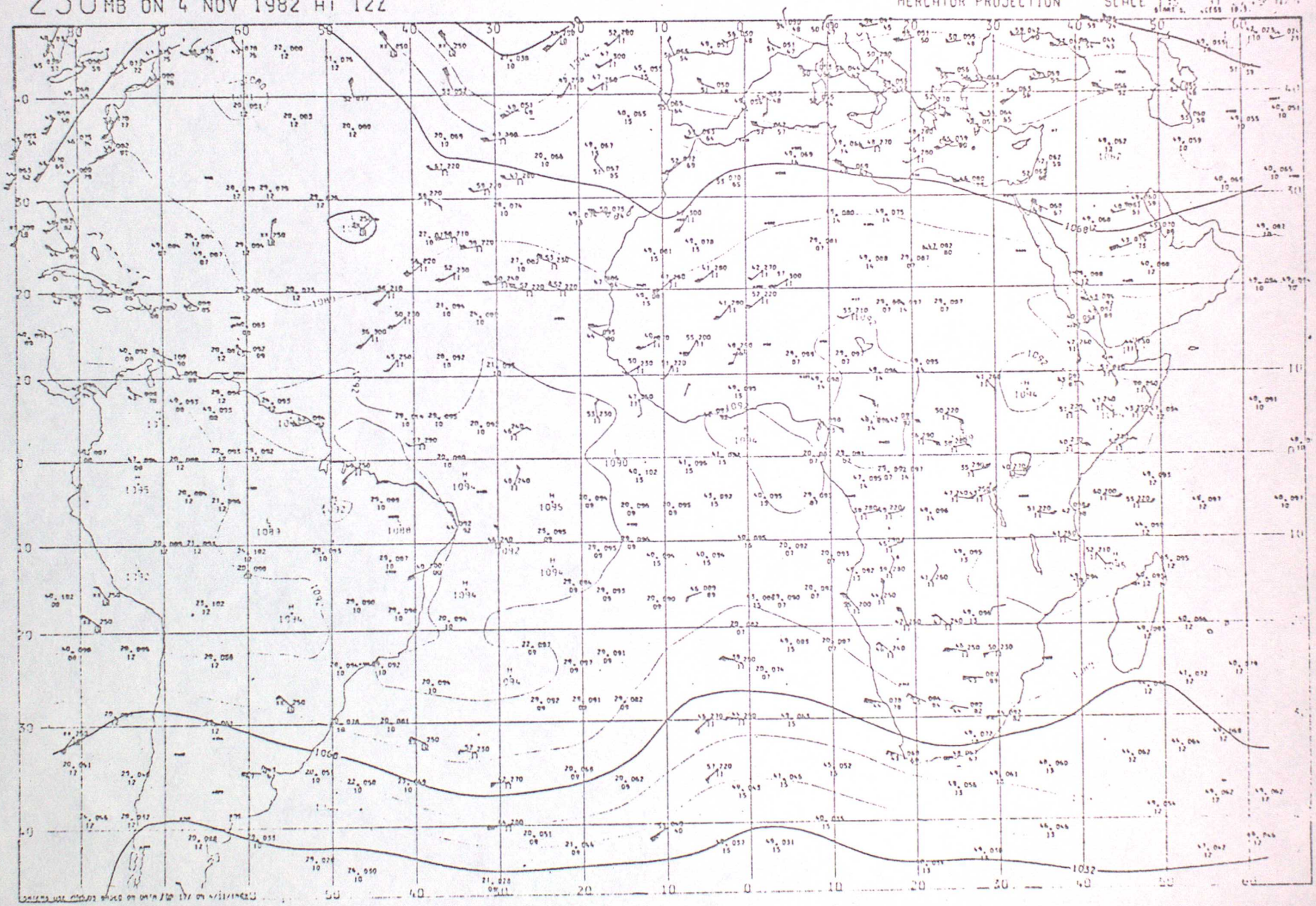

FIG. 26 (ii)

250 MB ON 4 NOV 1982 AT 12Z

MERCATOR PROJECTION SCALE 1:20.

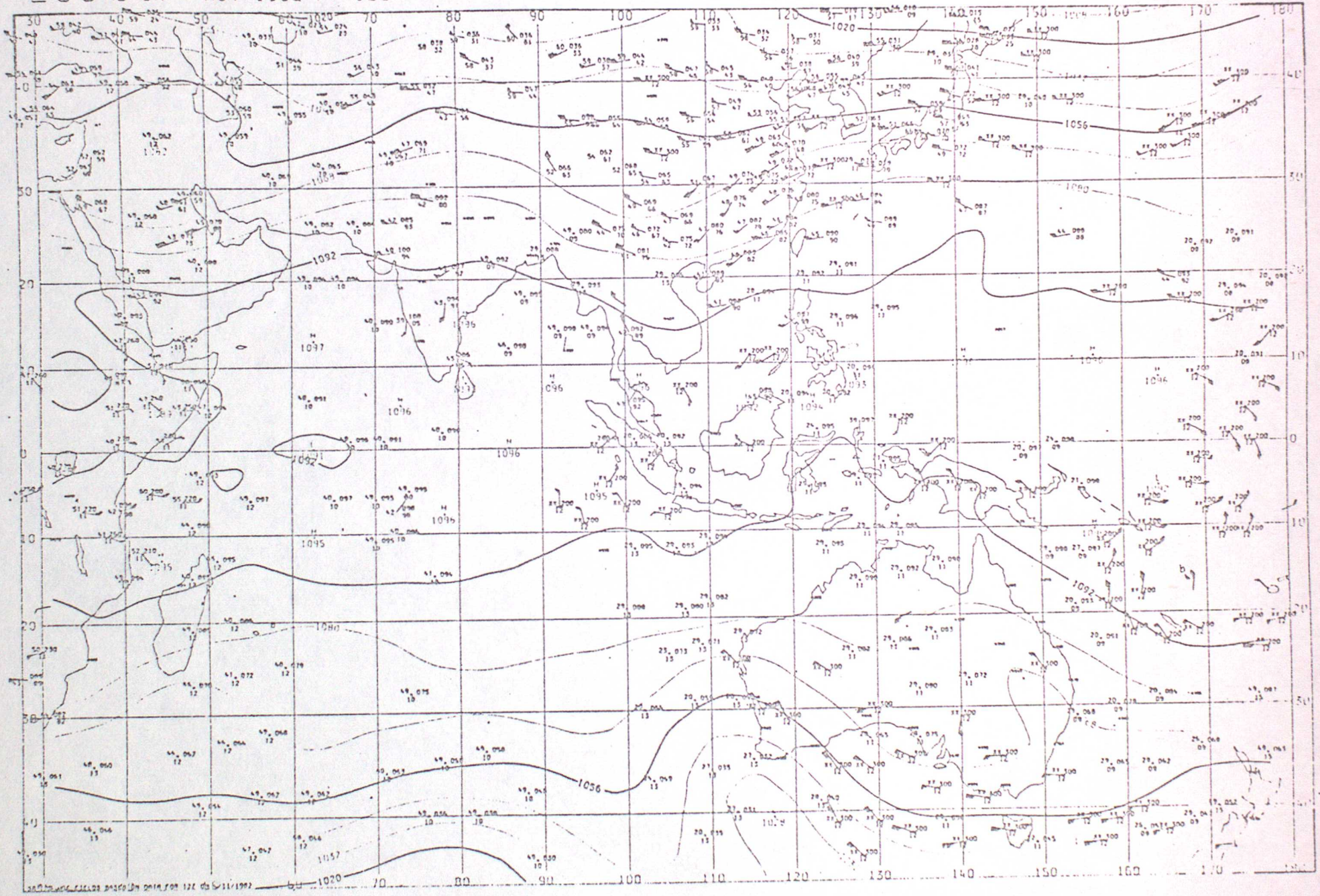

FIG. 26 (iii)

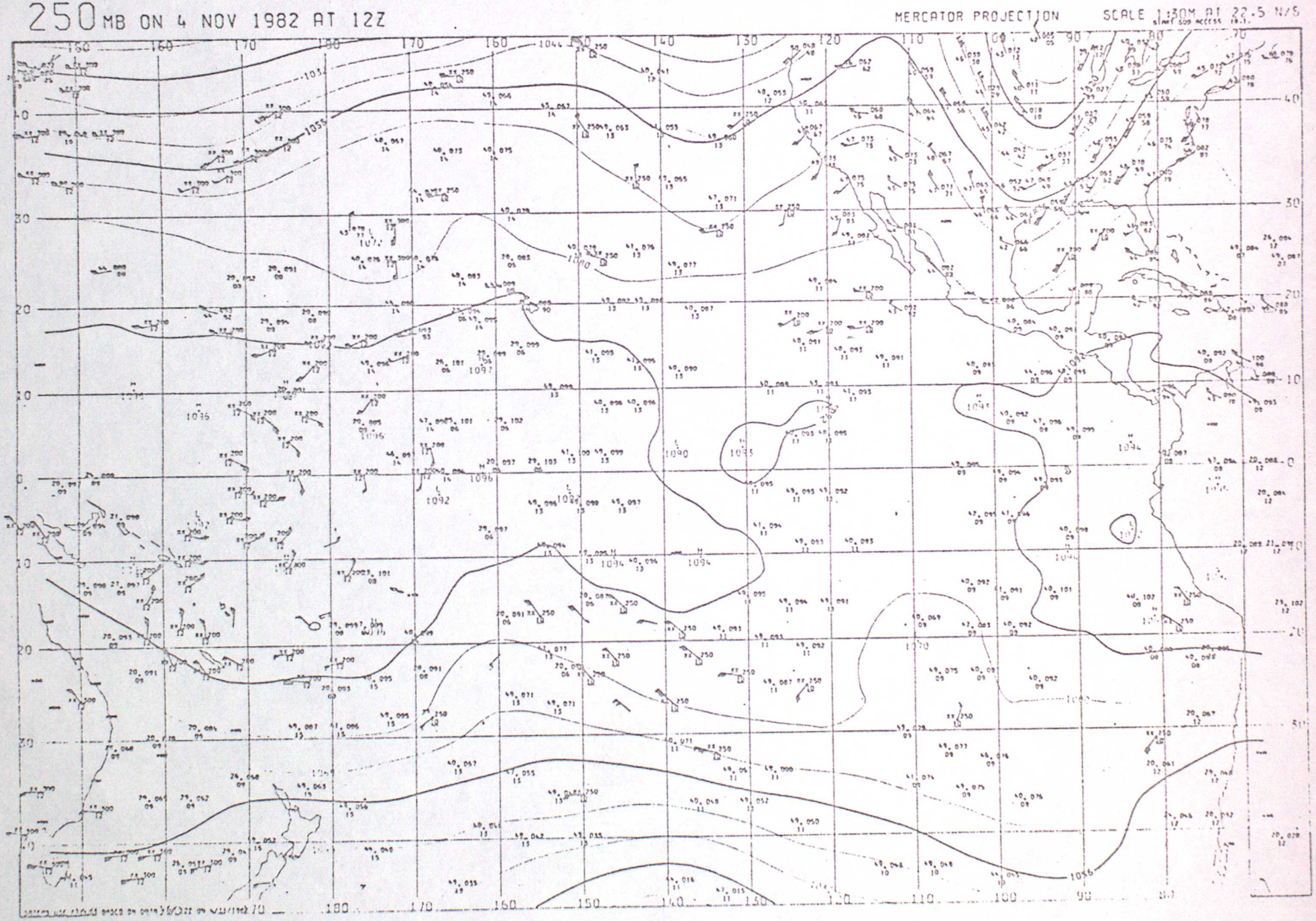
250 MB ON 4 NOV 1982 AT 12Z
MERCATOR PROJECTION
SCALE 1:30M AT 22.5 N/S

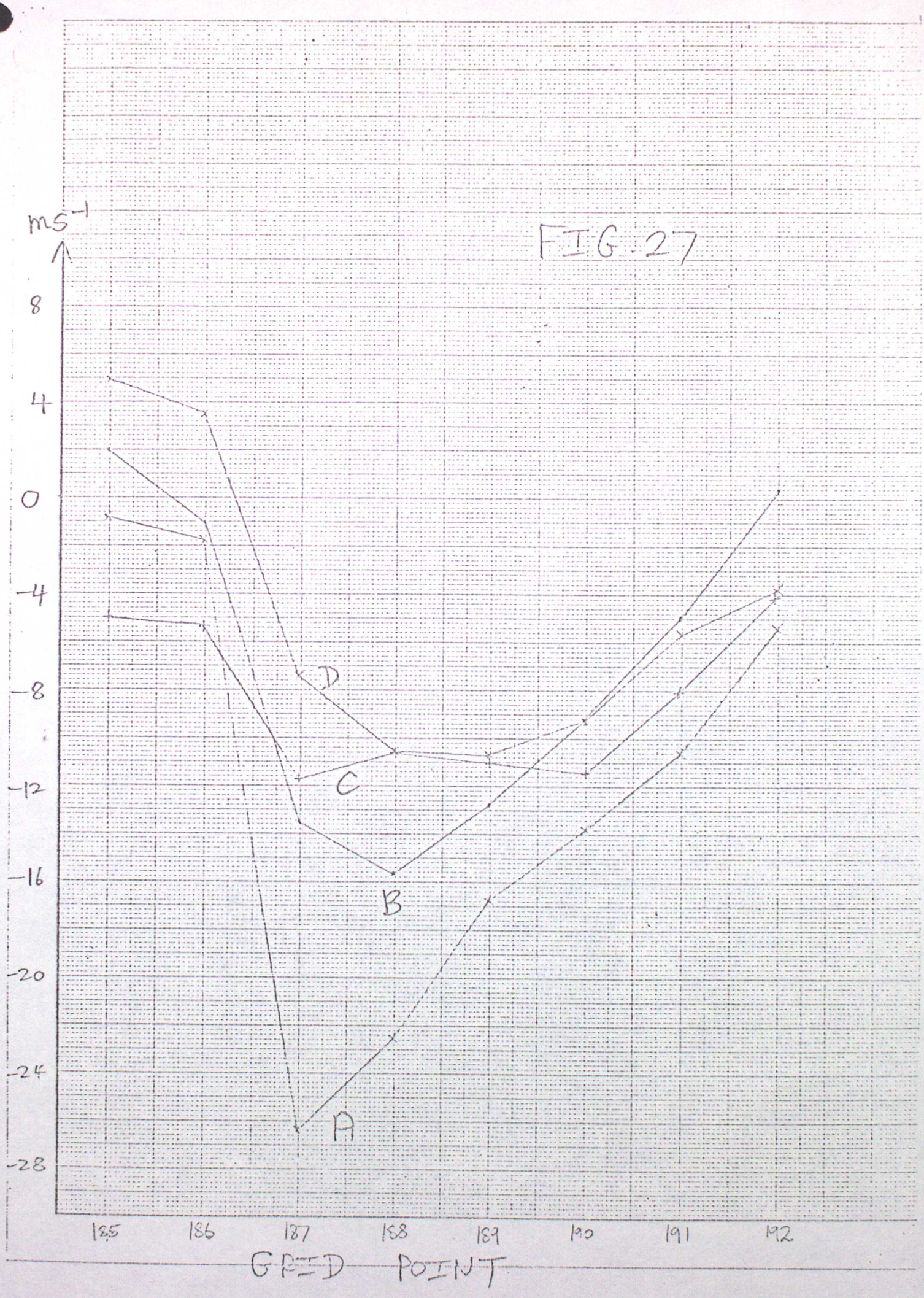
FIG:27
ms⁻¹
8
4
0
-4
-8
-12
-16
-20
-24
-28
185
186
187
188
189
190
191
192
GRID POINT
A
B
C
D

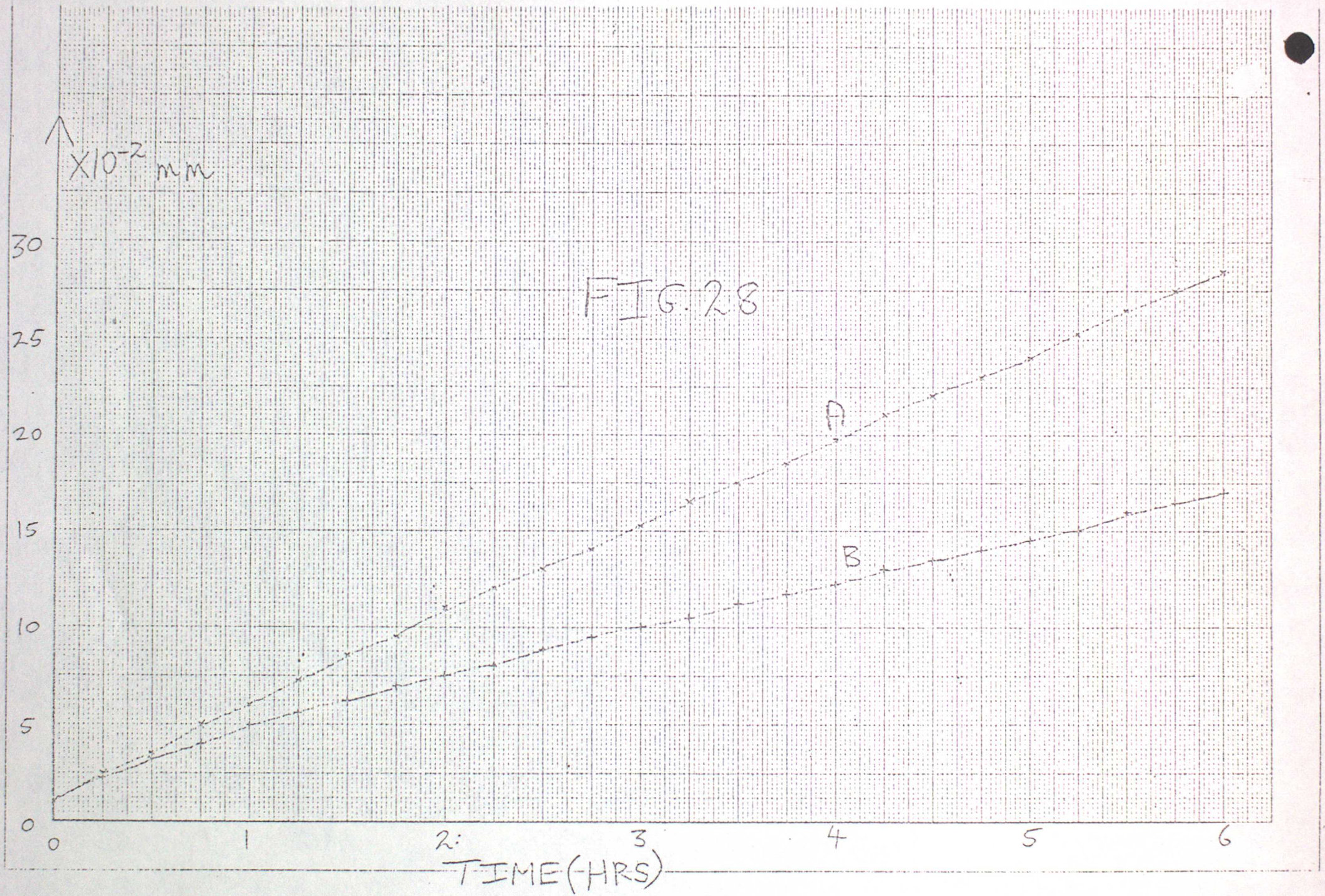

FIG. 28

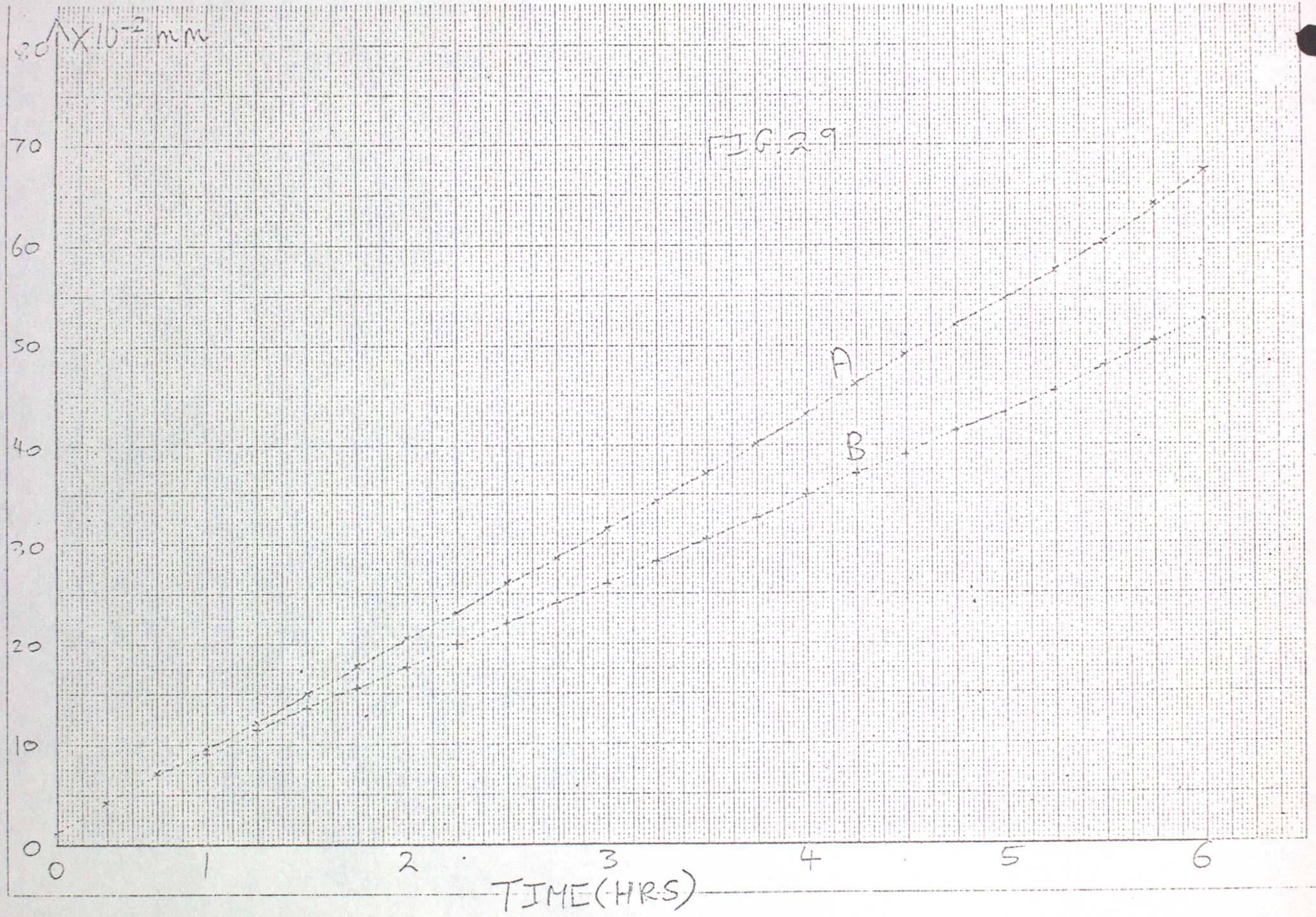

FIG: 29

FIG. 30

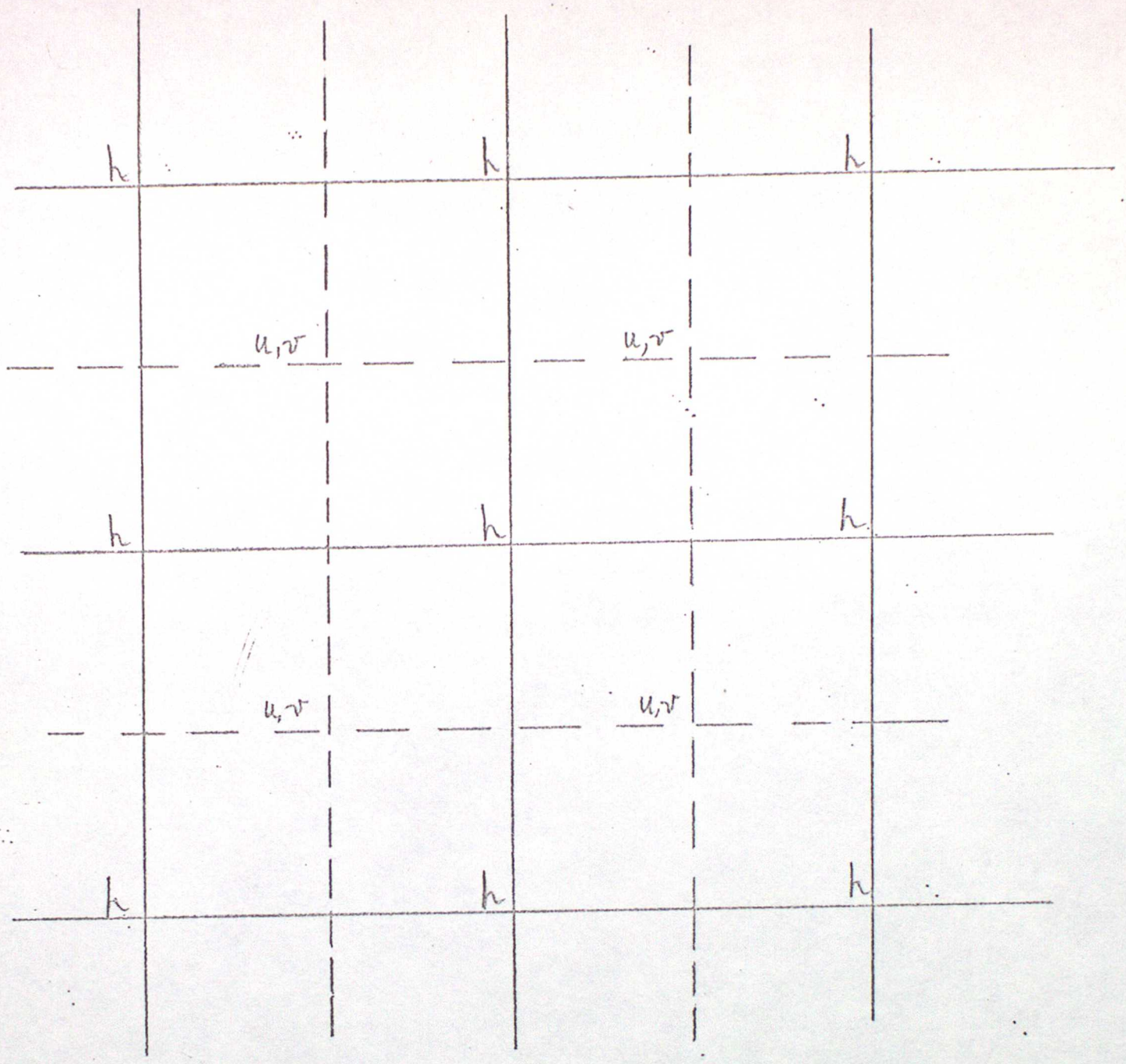

TABLE 1 GLOBAL RMS ERRORS OF ASSIMILATION

VARIABLE / RUN	p^* (mb)	θ ($^\circ$K)	$\underline{V}$ (Knots)	r (Kg/Kg x 10^{-3})
CONTROL	1.361	2.205	7.176	0.3937
ENHANCED DIFFUSION	1.325	2.159	6.732	0.3853
CONVENTIONAL DIVERGENCE DIFFUSION	1.288	2.101	6.484	0.3837

TABLE 2

RMS ERRORS

(i) 60N-30N

	PRESSURE BAND	p_s (mb)	θ (^{o}K)	$\underline{V}$ (Knots)	r ($Kg/Kg \times 10^{-3}$)
CONTROL	$350 \leq p$	1.400	1.296	5.798	0.4169
	$350 < p \leq 156$	1.400	2.741	11.14	0.03250
	$p < 156$	1.400	3.005	6.328	0.02110
ENHANCED DIFFUSION	$350 \leq p$	1.350	1.274	5.547	0.4038
	$350 < p \leq 156$	1.350	2.649	10.24	0.03196
	$p < 156$	1.350	2.960	6.032	0.02099
CONVENTIONAL DIVERGENCE DIFFUSION	$350 \leq p$	1.340	1.252	5.417	0.3979
	$350 < p \leq 156$	1.340	2.616	9.946	0.03248
	$p < 156$	1.340	2.779	6.128	0.02085

TABLE 2 RMS ERRORS

(ii) 30N-30S

	PRESSURE BAND	p^* (mb)	θ ($^\circ$K)	$\underline{V}$ (knots)	r (Kg/Kgx10^{-3})
CONTROL	$350 \leq p$	1.311	1.943	5.268	0.5498
	$350 < p \leq 156$	1.311	2.556	9.087	0.05624
	$p < 156$	1.311	3.133	6.861	0.007814
CONVENTIONAL DIVERGENCE DIFFUSION	$350 \leq p$	1.215	1.877	4.390	0.5584
	$350 < p \leq 156$	1.215	2.465	8.294	0.04769
	$p < 156$	1.215	2.959	6.470	0.007717

TABLE. 3 GLOBAL RMS ERRORS OF 24 HOUR FORECAST.

VARIABLE / FORECAST FROM	p_* (mb)	θ (^{o}K)	V (Knots)	r (Kg/Kgx10^{-3})
CONTROL	2.556	3.602	15.57	1.042
ENHANCED DIFFUSION	2.513	3.575	15.17	1.015
CONVENTIONAL DIVERGENCE DIFFUSION	2.512	3.508	14.96	1.014

TABLE 4

RMS ERRORS OF 24 HOUR FORECAST

60N-30N

	PRESSURE BAND	p^* (mb)	θ ($^\circ$K)	V (Knots)	r (Kg/Kgx10^{-3})
CONTROL	$350 \leq p$	2.578	2.404	12.09	0.92760
	$350 < p \leq 156$	2.578	4.309	21.23	0.05269
	$p < 156$	2.578	5.852	15.06	0.04370
ENHANCED DIFFUSION	$350 \leq p$	2.510	2.395	11.68	0.9045
	$350 < p \leq 156$	2.510	4.215	20.29	0.05350
	$p < 156$	2.510	6.013	14.03	0.04463
CONVENTIONAL DIVERGENCE DIFFUSION	$350 \leq p$	2.497	2.372	11.67	0.8949
	$350 < p \leq 156$	2.497	4.204	19.98	0.05182
	$p < 156$	2.497	5.876	13.81	0.04419

APPENDIX

Stablity Analysis

The stability analysis may be performed on a linearised version of the primitive equations with the divergence diffusion terms included. As shown by Temperton and Williamson (1979), the equations may be decoupled into N independent sets (N is the number of model levels). Since the divergence damping terms are added to the u and v momentum equations only, and are calculated from values of u and v at one level only, their presence does not affect the decoupling. The sets of equations obtained by this process are of the form:

$$\begin{aligned}
&\frac{\partial u_\nu}{\partial t} - F v_\nu + \frac{g}{a\cos\varphi}\frac{\partial h_\nu}{\partial \lambda} - \frac{\mu}{a\cos\varphi}\frac{\partial D_\nu}{\partial \lambda} = 0 \\
&\frac{\partial v_\nu}{\partial t} + F u_\nu + \frac{g}{a}\frac{\partial h_\nu}{\partial \varphi} - \frac{\mu}{a}\frac{\partial D_\nu}{\partial \varphi} = 0 \qquad \text{(A1)} \\
&\frac{\partial h_\nu}{\partial t} + \Lambda_\nu D_\nu = 0 \\
&\qquad\qquad \nu = 1, \ldots, N
\end{aligned}$$

where u_ν, v_ν etc are coefficients of the n-th vertical mode, $F = f + \frac{u \tan\varphi}{a}$, Λ_ν is a constant, and the other symbols have their usual meaning. The system is similar to the shallow water equations but with an extra terms for divergence diffusion. It can be noted in passing that the equations (A1) can be used to damp selected vertical modes.

A stability analysis may now be performed on the above system. For convenience the system is re-written in Cartesian co-ordinates:

$$\begin{aligned}
&\frac{\partial u}{\partial t} - Fv + g\frac{\partial h}{\partial x} - \mu\frac{\partial D}{\partial x} = 0 \\
&\frac{\partial v}{\partial t} + Fu + g\frac{\partial h}{\partial y} - \mu\frac{\partial D}{\partial y} = 0 \qquad \text{(A2)} \\
&\frac{\partial h}{\partial t} + HD = 0
\end{aligned}$$

where H represents a mean depth.

Centred space differencing and forward time differencing are the finite difference approximations used to solve (A2). To avoid a slight instability, treatment of the Coriolis term is made implicit. Hence using the notation:

$$\delta_x \Phi = [\Phi(x+d/2) - \Phi(x-d/2)]/d$$
$$\delta_y \Phi = [\Phi(y+d/2) - \Phi(y-d/2)]/d$$
$$\delta_t \Phi = [\Phi(t+\Delta t) - \Phi(t)]/\Delta t.$$
$$\overline{\Phi}^x = \tfrac{1}{2}[\Phi(x+d/2) + \Phi(x-d/2)]$$
$$\overline{\Phi}^y = \tfrac{1}{2}[\Phi(y+d/2) + \Phi(y-d/2)]$$

where Φ is any variable, $\Delta x = \Delta y = d$, then (A2) may be re-written:

$$\delta_t u - \tfrac{1}{2}F[v(t) + v(t+\Delta t)] + g\overline{\delta_x h}^y - \mu\overline{\delta_x D}^y = 0$$
$$\delta_t v + \tfrac{1}{2}F[u(t) + u(t+\Delta t)] + g\overline{\delta_y h}^x - \mu\overline{\delta_y D}^x = 0$$
$$\delta_t h + H\overline{D}^{xy} = 0 \qquad \text{(A3)}$$

These finite difference approximations are consistent with the staggering of the 'B' grid, as shown in Fig 30. The following substitutions are made:

$$\begin{pmatrix} u^n \\ v^n \\ h^n \end{pmatrix} = \begin{pmatrix} u_0 \\ v_0 \\ h_0 \end{pmatrix} \lambda^n e^{i(kl+ld)}$$

Taking u_0, v_0 , h_0 to be constants, and assuming $F = f$, then the following system results:

$$\left(\lambda - 1 + \frac{4\mu\Delta t}{d^2}\cos^2\frac{ld}{2}\sin^2\frac{kd}{2}\right)u_0 + \left\{\frac{\mu\Delta t}{d^2}\sin kd \sin ld - \tfrac{1}{2}f(\lambda+1)\Delta t\right\}v_0$$
$$+\frac{2g\Delta t\, i\lambda}{d}\sin\frac{kd}{2}\cos\frac{ld}{2}\,h_0 = 0$$

$$\left[\tfrac{1}{2}f(\lambda+1)\Delta t + \frac{\mu\Delta t}{d^2}\sin kd \sin ld\right]u_0 + \left[\lambda - 1 + \frac{4\mu\Delta t}{d^2}\cos^2\frac{kd}{2}\sin^2\frac{ld}{2}\right]v_0 \qquad \text{(A4)}$$
$$+\frac{2g\Delta t\, i\lambda}{d}\cos\frac{kd}{2}\sin\frac{ld}{2}\,h_0 = 0$$

$$\frac{2H\Delta t\, i}{d}\sin\frac{kd}{2}\cos\frac{ld}{2}\,u_0 + \frac{2iH\Delta t}{d}\sin\frac{ld}{2}\cos\frac{ld}{2}\,v_0 + (\lambda - 1)\,h_0 = 0$$

The condition for non-trivial solutions of the system (A4) is that the determinant of the matrix of coefficients should be zero. This condition results in the equation:

$$(\lambda-1)\left[(\lambda-1)^2+(\lambda-1)4A\Delta t(\mu+gH\Delta t)+4gH\Delta t^2A+f^2\Delta t^2(\lambda+1)^2\right]=0$$

where $$A=\frac{1}{d^2}\left(\sin^2\frac{kd}{2}\cos^2\frac{ld}{2}+\cos^2\frac{kd}{2}\sin^2\frac{ld}{2}\right)$$

Then $\lambda=1$ (neutrally stable solution) or

$$(\lambda-1)^2+(\lambda-1)4A\Delta t(\mu+gH\Delta t)+4gH\Delta t^2A+f^2\Delta t^2(\lambda+1)^2=0$$

Re-arranging this and putting $f_1=f/2$ gives:

$$\lambda^2(1+f_1^2\Delta t^2)+2\lambda(2AgH\Delta t^2+f_1^2\Delta t^2+2A\Delta t\mu-1)$$
$$+1+f_1^2\Delta t^2-4\mu A\Delta t=0$$

The solution for λ is then:

$$\lambda=\left[1-f_1^2\Delta t^2-2A\Delta t(\mu+gH\Delta t)\right](1+f_1^2\Delta t^2)^{-1}$$
$$\pm\left\{\left[2A\Delta t(\mu+gH\Delta t)+f_1^2\Delta t^2-1\right]^2-(1+f_1^2\Delta t^2)(1+f_1^2\Delta t^2-4\mu A\Delta t)\right\}^{\frac{1}{2}}(1+f_1^2\Delta t^2)$$

Suppose

$$\left[2A\Delta t(\mu+gH\Delta t)+f_1^2\Delta t^2-1\right]^2\leq(1+f_1^2\Delta t^2)(1+f_1^2\Delta t^2-4\mu A\Delta t) \qquad (A5)$$

then

$$|\lambda|^2=1-\frac{4\mu A\Delta t}{1+f_1^2\Delta t^2}\leq 1$$ since $\mu\geq 0, A\geq 0$.

which gives a stable solution. The inequality (A5) may be written:

$$\left[A\Delta t(\mu+gH\Delta t)-1\right]\left[A\Delta t(\mu+gH\Delta t)+f_1^2\Delta t^2\right]\leq-\mu A\Delta t(1+f_1^2\Delta t^2)$$

(A6)

Since $\mu, A \geq 0$ then

$$[A\Delta t(\mu+gH\Delta t)-1][A\Delta t(\mu+gH\Delta t)+f_1^2\Delta t^2] \leq 0$$

Since the right hand operand is non-negative, the following condition for stable solutions results:

$$A\Delta t(\mu+gH\Delta t) \leq 1$$

A sufficient condition for all wavenumbers is given by:

$$A_{max}\Delta t(\mu+gH\Delta t) \leq 1$$

where A_{max} is the maximum value of A for the range of wavenumbers permitted on the 'B' grid. The above inequality yeilds:

$$\mu \leq \frac{1}{A_{max}\Delta t} - gH\Delta t = \frac{1}{A_{max}\Delta t} - c^2\Delta t \qquad (A7)$$

where c is the phase speed of a gravity wave on a non-rotating earth. Upper and lower bounds on A may be obtained from the following identity:

$$A = \frac{1}{d^2}\left(\sin^2\frac{kd}{2}\cos^2\frac{ld}{2} + \cos^2\frac{kd}{2}\sin^2\frac{ld}{2}\right)$$

$$= \frac{1}{d^2}\left(1 - \sin^2\frac{ld}{2}\sin^2\frac{kd}{2} - \cos^2\frac{kd}{2}\cos^2\frac{ld}{2}\right)$$

Hence $0 \leq A \leq \frac{1}{d^2}$

Putting $A_{max} = \frac{1}{d^2}$, we have

$$\mu \leq \Delta t\left(\frac{d^2}{\Delta t} - c^2\right) \qquad (A8)$$

as a sufficient condition for stability. Note that the upper bound for μ reduces as the phase speed increases. In order to obtain a sufficient condition

for stability the phase speed of the fastest moving wave (the external gravity wave) is used in (A8). The equivalent depth of the external mode in the current operational model is taken to be 9.8846 Km (Temperton, private communication) and using this the phase speed for the external mode on a non-rotating earth is approximately 311 ms^{-1}.